CellPress

Cell Host & Microbe
Article

A Plant Phosphoswitch Platform Repeatedly Targeted by Type III Effector Proteins Regulates the Output of Both Tiers of Plant Immune Receptors

Eui-Hwan Chung,[1] Farid El-Kasmi,[1] Yijian He,[1,6] Alex Loehr,[1,7] and Jeffery L. Dangl[1,2,3,4,5,*]
[1]Department of Biology
[2]Curriculum in Genetics and Molecular Biology
[3]Carolina Center for Genome Sciences
[4]Department of Microbiology and Immunology
University of North Carolina, Chapel Hill, Chapel Hill, NC 27599, USA
[5]Howard Hughes Medical Institute, University of North Carolina, Chapel Hill, Chapel Hill, NC 27599, USA
[6]Present address: Department of Plant Pathology, NC State University, Raleigh, NC 27695-7616, USA
[7]Present address: New York Medical College, School of Medicine, Valhalla, NY 10595, USA
*Correspondence: dangl@email.unc.edu
http://dx.doi.org/10.1016/j.chom.2014.09.004

SUMMARY

Plants detect microbes via two functionally interconnected tiers of immune receptors. Immune detection is suppressed by equally complex pathogen mechanisms. The small plasma-membrane-tethered protein RIN4 negatively regulates microbe-associated molecular pattern (MAMP)-triggered responses, which are derepressed upon bacterial flagellin perception. We demonstrate that recognition of the flagellin peptide MAMP flg22 triggers accumulation of RIN4 phosphorylated at serine 141 (pS141) that mediates derepression of several immune outputs. RIN4 is targeted by four bacterial type III effector proteins, delivered temporally after flagellin perception. Of these, AvrB acts with a host kinase to increase levels of RIN4 phosphorylated at threonine 166 (pT166). RIN4 pT166 is epistatic to RIN4 pS141. Thus, AvrB contributes to virulence by enhancing "rerepression" of immune system outputs. Our results explain the evolution of independent effectors that antagonize accumulation of RIN4 pS141 and of a specific plant intracellular NLR protein, RPM1, which is activated by AvrB-mediated accumulation of RIN4 pT166.

INTRODUCTION

Plants evolved a two-tiered immune receptor system to respond to microbial infection. At the plasma membrane (PM), plant pattern-recognition receptors (PRRs) recognize common microbe-associated molecular patterns (MAMPs). Subsequent intracellular signal transduction results in MAMP-triggered immunity (MTI), which can halt microbial proliferation. Pathogens circumvent PRR-mediated MTI by delivering virulence effectors to block it, contributing to effector-triggered susceptibility (ETS) (Dodds and Rathjen, 2010 ; Feng and Zhou, 2012; Jones and Dangl, 2006). For example, type III effectors (T3Es) from Gram-negative phytopathogenic bacteria are injected into plant cells via the type III secretion system. Many T3Es are enzymes or enzyme mimics that alter host defense to facilitate pathogen survival by dampening or suppressing MTI. Plants therefore evolved a highly polymorphic second tier of intracellular nucleotide-binding domain leucine-rich repeat (NLR) immune receptors. Some of these can be activated by "modified-self" products of T3E action to reboot and amplify the suppressed MTI response, resulting in effector-triggered immunity (ETI) (Dodds and Rathjen, 2010; Jones and Dangl, 2006). Independently evolved effectors from different kingdoms (bacteria, fungi, and oomycetes) can interact with shared sets of host proteins (Mukhtar et al., 2011). Thus, pathogens need to evolve sufficiently diverse effector repertoires to ensure that these can collectively dampen MTI, while plants only need to be right once: evolution of a single NLR that can sense effector manipulation of a host target is typically sufficient to initiate ETI.

Perception of MAMPs by PRRs induces MTI (Belkhadir et al., 2014; Macho and Zipfel, 2014). The prototypic PRR kinase, flagellin-sensitive 2 (FLS2) from *Arabidopsis* perceives a conserved N-terminal epitope of flagellin, flg22. Flg22 recognition induces heteromerization of FLS2 with a multifunctional coreceptor, Brassinosteroid insensitive 1-associated kinase 1 (BAK1) to initiate MTI via reciprocal activation of FLS2, BAK1, and subsequent signaling. FLS2 activation (5–10 min post-ligand binding) leads to commonly assayed MTI output branches resulting in a reactive oxygen species (ROS) burst, MAP kinase activation, transcriptional reprogramming (by ~30–60 min), and cell wall lignification exemplified by callose deposition.

RPM1-interacting protein 4 (RIN4) is a small, unstructured protein that is acylated into the PM. RIN4 is a negative regulator of MTI (Kim et al., 2005). Multiple T3Es that target RIN4 and suppress MTI are delivered into plant cells ~60–90 min after infection (Grant et al., 2000; Huynh et al., 1989), a time point when MTI signaling is well underway. These include AvrRpm1, AvrB, AvrRpt2, and HopF2 (Axtell and Staskawicz, 2003; Mackey et al., 2003; Mackey et al., 2002; Wilton et al., 2010). Logically, these interactions should enhance RIN4-dependent negative regulation of MTI, but no mechanism for this has been described. AvrRpm1 and AvrB are delivered into host cells,

where they target and modify RIN4 at the PM (Nimchuk et al., 2000). AvrRpm1 and AvrB activity leads to RIN4 hyperphosphorylation, though neither are kinases, and activation of the NLR receptor RPM1 when it is present. AvrRpt2 is a cysteine protease (Coaker et al., 2005), and it cleaves RIN4 at the PM, thus activating the RPS2 NLR when it is present (Axtell and Staskawicz, 2003; Mackey et al., 2003). It is not known how the ADP-ribosyl transferase activity of HopF2 (Wang et al., 2010) modulates RIN4. Its presumed modification of RIN4 is not yet associated with activation of an NLR receptor. All of these T3Es have, or are likely to have, additional cellular targets.

A small subset of related PM-associated receptor-like cytoplasmic kinases (RLCKs; family VII) can phosphorylate RIN4. In particular, RIPK phosphorylates RIN4 T21, S160, and the evolutionarily invariant RIN4 T166 (Liu et al., 2011). AvrB enhances RIPK activity by an unknown mechanism (Chung et al., 2011; Liu et al., 2011). Phosphomimic derivatives RIN4 T166D/E drive effector-independent activation of RPM1, and nonphosphorylable RIN4 T166A cannot support effector-mediated RPM1 activation (Chung et al., 2011). Thus, a plausible untested model is that AvrB and AvrRpm1 contribute to pathogen virulence by enhancing RIPK-dependent accumulation of RIN4 pT166 (Chung et al., 2011). Close relatives of RIPK are irreversibly inactivated by additional bacterial T3Es, and this can inhibit RPM1 activation (Feng et al., 2012), further suggesting that regulation of RIN4 phosphorylation may have been repeatedly targeted during pathogen evolution.

While these results added significantly to our understanding of RPM1 activation, they did not explain how AvrB, or any of the other T3E targeting RIN4, contributes to suppression of MTI in plants naturally lacking *RPM1* (Rose et al., 2012). We demonstrate that RIN4 is a "phosphoswitch" that regulates common outputs of PRR-dependent MTI; that the critical phosphorylation event for this is RIN4 pS141; and that at least AvrB and AvrRpm1, and potentially HopF2, contribute to MTI by antagonizing the accumulation of RIN4 pS141. Our results specify functional constraints on the as-yet-undiscovered kinase that phosphorylates RIN4 pS141.

RESULTS

RIN4 S141 Contributes to MTI

RIN4 amino acids S47 and S141 were noted as phosphorylation sites in shotgun PM phosphoproteomic surveys following stimulation by flg22 (Benschop et al., 2007; Nühse et al., 2004, 2007) (Figure S1A, red arrow, available online). We aligned RIN4 orthologous sequences from other plant genomes and noted that S47 is not well conserved. In contrast, positions orthologous to RIN4 S141 are, with three exceptions, serine or threonine, and are thus a plausible evolutionarily conserved phosphorylation site (Figures S1B–S1D). The functionally critical RIPK target site, RIN4 T166, is conserved across all sequenced plant genomes surveyed (Figure S1D) (Chung et al., 2011).

To address whether S47 and S141 are required for RIN4 function during MTI, we generated transgenic plants expressing either T7-epitope-tagged wild-type RIN4 or single and *cis* double point mutations at these positions expressed from the native *RIN4* promoter. We substituted S47 and S141 to alanine (A), to block phosphorylation, or to glutamate (E), to mimic phosphorylation at each position. The recipient plants were *rpm1 rps2 rin4* triple mutants, which allowed us to assess complementation of RIN4 function in MTI in the absence of confounding ETI activation through the RPM1 or RPS2 NLR proteins. We used homozygous transgenic lines that expressed comparable levels of T7-epitope-tagged RIN4 (hereafter, wild-type RIN4) and RIN4 mutant derivatives in our assays (Figure S1B).

We assessed whether RIN4 S47 or S141 were required for negative regulation of MTI. We counted flg22-induced callose deposition in leaves of transgenic plants expressing the RIN4 S47A and S141A single or *cis* double point mutants (Figure S1B). Figures 1A and 1B show that flg22-induced callose deposition in wild-type Col-0 was *FLS2* dependent, as expected. The *rpm1 rps2 rin4* parent line was hyperresponsive to flg22 in this assay, consistent with negative regulation of MTI by RIN4 (Kim et al., 2005) that was restored by complementation with wild-type *RIN4*. Importantly, plants expressing RIN4 S141A in either a single or *cis* double mutant context accumulated significantly less callose than plants expressing wild-type *RIN4*, thus resembling the *rin4*-null allele (Figure 1A). Conversely, plants expressing RIN4 S141E single or *cis* double mutants accumulated significantly more callose in response to flg22 than plants complemented with wild-type RIN4 (Figure 1B), though not as much as the parental *rpm1 rps2 rin4* line. We did not attribute any function in flg22-driven callose deposition to RIN4 S47 in these experiments.

Pretreatment of Col-0 leaves with flg22 activates biologically relevant MTI, assayed as suppressed proliferation of the virulent pathogen *Pseudomonas syringae* pv. *tomato* strain *Pto* DC3000 inoculated 24 hr later (Zipfel et al., 2004); this was *FLS2* dependent (Figure 1C). The *rpm1 rps2 rin4* parent did not express a phenotype different than Col-0 in this assay, suggesting that flg22-dependent induction of MTI can proceed in the absence of RIN4. However, the expression of RIN4 S141A single or *cis* double mutant combinations could not support full flg22-dependent induction of MTI (Figure 1C). Expression of RIN4 S141E single or *cis* double mutants retained this function (Figure 1C). These results demonstrate that flg22-induced MTI tolerated loss of RIN4, or phosphomimic mutation at RIN4 S141, but not loss of the phospho-site. This is consistent with a requirement for RIN4 S141 phosphorylation in the induction of flg22-dependent MTI as measured in this assay. Because Figures 1A and 1B demonstrate that there is no function for S47E in the tested MTI outputs, we focused our analyses on RIN4 S141 derivatives.

We monitored additional common and temporally separable MTI outputs including flg22-induced ROS production, MAP kinase activation, and early marker gene expression (Chinchilla et al., 2007; Schwessinger et al., 2011). We monitored the ROS burst following treatment with flg22 (Figure 1D; Experimental Procedures). The flg22 response of *rpm1 rps2 rin4* was consistently slightly faster and of marginally higher amplitude than wild-type; this line complemented with RIN4 S141E responded with wild-type kinetics and marginally higher amplitude, and RIN4 S141A was essentially wild-type. These differences were reproducible, though not statistically significant. We observed no remarkable differences in the timing or amplitude of MAPK activation, with the exception that plants expressing RIN4 S141A exhibited slightly less MAPK activation than those expressing wild-type RIN4 or RIN4 S141E (Figure 1E). We selected

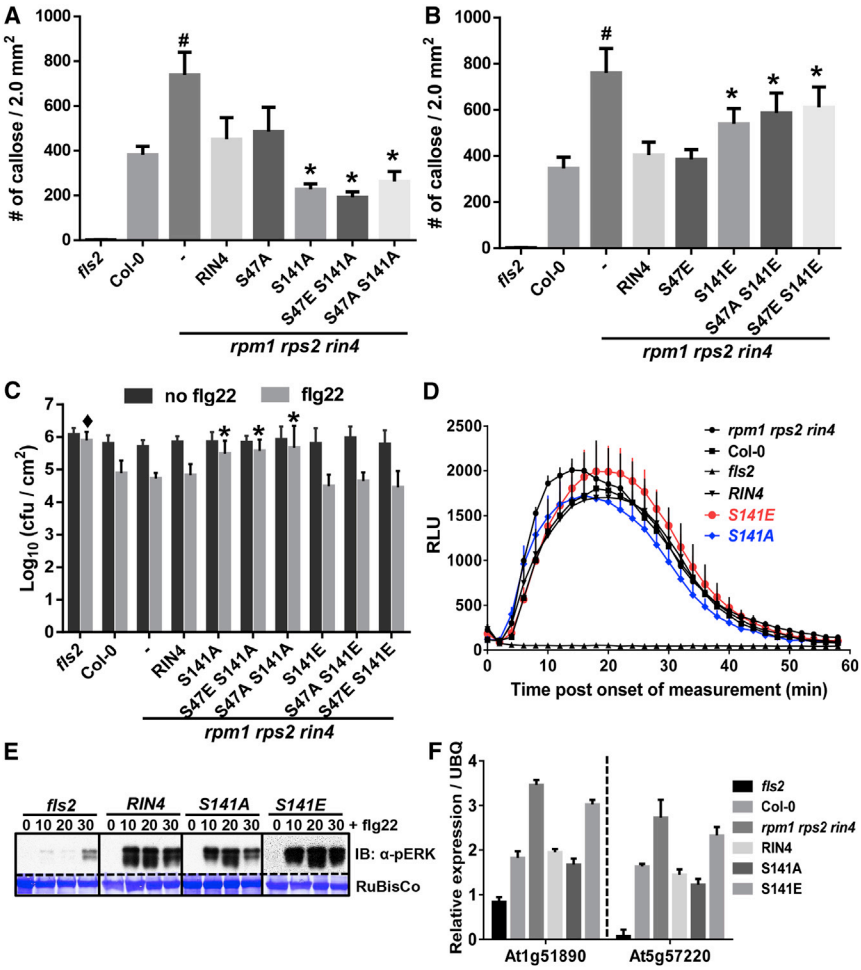

Figure 1. RIN4 S141 Contributes to MTI

(A) Suppressed callose accumulation in *rpm1 rps2 rin4* plants expressing T7-tagged phospho-dead RIN4 S47A or S141A derivatives (from the native *RIN4* promoter here and in all cases below, except as noted) compared to wild-type in response to flg22. Induced callose deposition was monitored in 16 independently treated plant samples (n = 16) 18 hr after infiltration of 1 μM flg22. Callose deposition sites here and throughout were counted in a position-standardized view of 2 mm^2. Error bar represents 2 × SE. Pair-wise comparisons for all means of transgenic plants expressing RIN4 mutants S47A, S141A, S47E S141A, and S47A S141A compared to those expressing RIN4 wild-type were examined by one-way ANOVA test followed by Tukey-Kramer HSD with 95% confidence (asterisks; *). Number sign (#) denotes significant difference compared to Col-0 using a one-way ANOVA test followed by Tukey-Kramer HSD with 95% confidence. Similar results were obtained from four independent replicates.

(B) Enhanced callose accumulation in *rpm1 rps2 rin4* plants expressing T7-tagged phosphomimic RIN4 S47E or S141E derivatives compared to wild-type in response to flg22. Callose deposition was assayed as in (A). A one-way ANOVA test followed by Tukey-Kramer HSD with 95% confidence was used to compare plants expressing wild-type RIN4 to those expressing RIN4 mutants S47E, S141E, S47A S141E, and S47E S141E (asterisks; *). Number sign (#) denotes significant difference compared to Col-0 using a one-way ANOVA test followed by Tukey-Kramer HSD with 95% confidence. Note that (A) and (B) are from the same experiment and that the first three control samples in (B) are the same data as in (A). Similar results were obtained from four independent replicates.

(C) flg22-activated bacterial growth suppression in *rpm1 rps2 rin4* plants expressing T7-tagged wild-type RIN4, RIN4 S47, or RIN4 S141-derived missense mutants. A solution of 100 nM flg22 was infiltrated 24 hr prior to inoculation with 1 × 10^5 cfu/ml *Pto* DC3000(EV). Bacterial growth was monitored 3 days postinoculation (gray bar). Plants preinfiltrated with water were used as a negative control for flg22 pretreatment (black bar). Error bar represents 2 × SE (n = 16). Asterisks (*) indicate significant difference compared to wild-type RIN4 analyzed by one-way ANOVA test with Tukey-Kramer HSD with 95% confidence. Similar results were obtained from four independent experiments.

(D) ROS burst in Col-0, *fls2*, *rpm1 rps2 rin4*, and *rpm1 rps2 rin4* plants expressing T7-tagged wild-type RIN4, RIN4 S141A, or RIN4 S141E. Luminol assay was conducted as described in Experimental Procedures after 100 nM flg22 treatment. Data were collected from 12 individual leaf discs (n = 12 per genotype) with four independent replicates. Error bars represent 2 × SE.

(E) MPK activation in Col-0, *fls2*, *rpm1 rps2 rin4*, and *rpm1 rps2 rin4* plants expressing T7-tagged wild-type RIN4, RIN4 S141A, or RIN4 S141E. Five-week old plants of each genotype were infiltrated with 100 nM flg22 and sampled at 10, 20, and 30 min posttreatment. A total of 30 μg of total protein was loaded for immunoblot with α-pERK to detect active MPKs. Coomassie brilliant blue (CBB) staining of RuBisCo demonstrates equal loading.

(F) Early defense gene expression in response to 1 μM flg22 infiltration in Col-0, *fls2*, *rpm1 rps2 rin4*, and *rpm1 rps2 rin4* plants expressing T7-tagged wild-type RIN4, RIN4 S141A, or RIN4 S141E. Gene expression for *At1g51890* and *At5g57220* normalized to *UBQ10* expression (endogenous control) was analyzed by quantitative RT-PCR on RNA harvested 3 hr post flg22 treatment. Error bars represent 2 × SE (n = 3). Similar results were observed in two independent repeats.

the early defense marker genes *At1g51890* and *At5g57220* for quantitative RT-PCR analysis at 3 hr post-flg22 treatment (Schwessinger et al., 2011) (Experimental Procedures). The flg22-dependent expression levels for each defense gene in Col-0 was *FLS2* dependent, enhanced in *rpm1 rps2 rin4*, consistent with negative regulation of MTI by RIN4 (Kim et al., 2005), and complemented by wild-type RIN4. Notably, RIN4 S141E-expressing plants supported enhanced defense gene expression that essentially phenocopied the *rin4* null in the *rpm1 rps2 rin4* parent. The RIN4 S141A plants, by contrast, were wild-type for this function (Figure 1F).

Together, our survey of several temporally diverse and separable MTI outputs demonstrates that RIN4 S141 is a functionally relevant phosphorylation site and that RIN4 S47 is not, at least for the outputs measured. RIN4 S141 is required for at least maximal restriction of bacterial pathogen growth and callose deposition and contributes to ROS burst and defense gene induction. This differential requirement likely reflects quantitative contributions of RIN4 pS141 to each MTI output, since a RIN4 S141 phosphomimic is sufficient to enhance at least flg22-induced callose accumulation and early defense gene expression.

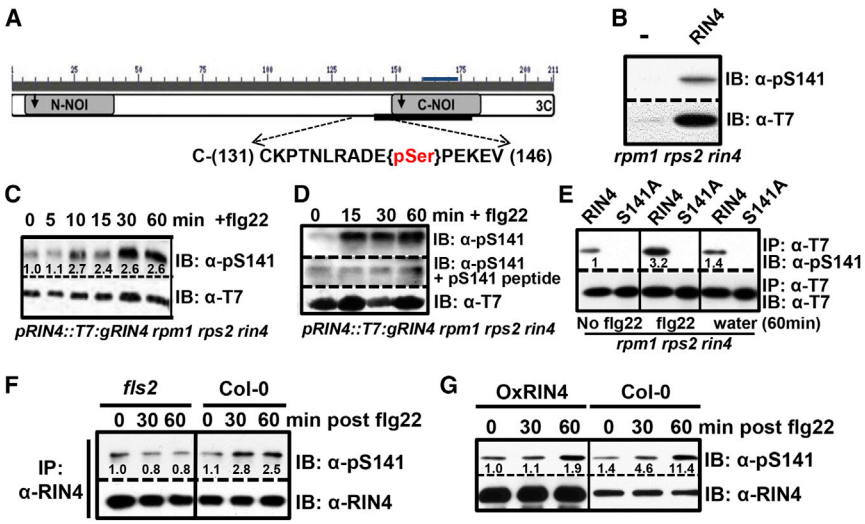

Figure 2. Phosphorylation of RIN4 S141 Is Induced by flg22

(A) Schematic diagram positioning the RIN4 S141 phosphopeptide used to generate phospho-specific antibody (α-pS141). The RIN4 N- and C-terminal NOI domains are noted as gray boxes and, downward arrows are the AvrRpt2 cleavage sites. Phosphopeptide-specific antibody was raised against a peptide spanning positions 131–146 of the RIN4 sequence. The AvrB binding site (Desveaux et al., 2007) is denoted by a thick black bar, and the previously described phosphopeptide used to produce specific antisera against pT166 is shown as a thin blue bar (positions 155–168; Chung et al., 2011).

(B) Specificity of RIN4 α-pS141 antisera. Whole-cell extracts from leaves of *rpm1 rps2 rin4* and transgenic *rpm1 rps2 rin4* plants expressing T7-tagged wild-type RIN4 were immunoblotted with α-pS141 or α-T7 antisera. Thirty micrograms of total protein was loaded.

(C) Flg22-induced phosphorylation of RIN4 pS141. Leaves from 5-week old transgenic plants from (B) were infiltrated with 1 μM of flg22 and sampled at the indicated time points. Whole-cell extracts were probed with α-pS141. Equal loading was demonstrated by immunoblot with α-T7 after stripping the membrane used for the α-pS141 blot. One of three independent replicates with similar results.

(D) Peptide competition confirms specific RIN4 S141 phosphorylation following flg22 recognition. Immunoblot of samples collected as in (B) and (C) with α-pS141 was performed with and without preincubation of whole-cell extracts with 3 μM phosphopeptide pS141 (CKPTNLRADEpSPEKEV) prior to α-pS141 detection. As in (C), an α-T7 blot measuring steady-state RIN4 levels was used as a loading control.

(E) Steady-state and flg22-dependent phosphorylation of RIN4 on S141 is specific. Transgenic plants expressing T7-tagged wild-type RIN4 or the RIN4 S141A mutant were infiltrated with 1 μM flg22 or water or not infiltrated. Samples were harvested at 60 min posttreatment. Numbers in the α-pS141 blot lanes represent the relative expression levels of RIN4 pS141 compared to the respective α-T7 loading control blot. Similar results were observed in three independent repeats.

(F) RIN4 S141 phosphorylation is FLS2 dependent. Immunoprecipitation with α-RIN4 from *fls2* and Col-0 plants was performed followed by immunoblots with α-RIN4 and α-pS141. Samples were collected 0, 30, and 60 min after treatment with 1 μM of flg22. Three independent experiments displayed similar results.

(G) RIN4 S141 phosphorylation in Col-0 and OxRIN4 in Col-0 post flg22-treatment. Immunoblots with α-RIN4 and α-pS141 from Col-0 and OxRIN4 were performed with 20 μg of total protein extracts of each genotype. Samples were collected 0, 30, and 60 min after treatment with 1 μM of flg22 48 hr postinduction of RIN4 expression by 20 μM dexamethasone. Two independent experiments displayed similar result.

RIN4 S141 Phospho-Status Does Not Alter Effector-Dependent Activation of the RPM1 or RPS2 NLRs

Because RIN4 S141 mutations alter MTI outputs, we tested whether S141 mutations influenced the ability of AvrB or AvrRpm1 to activate RPM1. We infiltrated *Pto* DC3000(*avrB*) or *Pto* DC3000(*avrRpm1*) into leaves of a second set of comparable expression transgenic lines expressing wild-type RIN4 or S47 or S141 single and *cis* double mutants, using as a parent either our *rpm1 rps2 rin4 pRPM1::RPM1-myc* line (Chung et al., 2011) or *rpm1 rps2 rin4* as the control. Mutations at RIN4 S47 or S141 had no reproducible effect on RPM1 activation with either effector (Figures S2A–S2C). In addition, AvrRpt2-dependent cleavage of RIN4 occurred in leaves of these transgenic plants following infiltration of *Pto* DC3000(*avrRpt2*) (Figure S2D). This is a required step for RPS2 activation (Axtell and Staskawicz, 2003; Coaker et al., 2005; Mackey et al., 2003). Hence, we conclude that the RIN4 S141 relevant phenotypes defined in Figure 1 do not alter either RPM1 activation or, presumably, RPS2 activation.

Phosphorylation of RIN4 S141 Is Induced by flg22

We generated a phosphopeptide-specific antibody (α-pS141) to detect site-specific phosphorylation after flg22 treatment (Figure 2A). We performed immunoblots on leaf extracts of *rpm1 rps2 rin4* and *pRIN4::T7-RIN4 rpm1 rps2 rin4* plants to demonstrate the specificity of the α-pS141 serum (Figure 2B). RIN4 was detected only in leaf extracts expressing T7-RIN4, but not in the *rpm1 rps2 rin4* parent, like the control blot with α-T7 (Figure 2B). We investigated induction of RIN4 pS141 accumulation in leaves of transgenic plants expressing wild-type RIN4 sampled at 0, 5, 10, 15, 30, and 60 min post-flg22 infiltration. We chose these time points from knowledge of global flg22-dependent transcriptional responses (Schwessinger et al., 2011) and our data showing robust steady-state defense gene mRNA accumulation at 3 hr post-flg22 treatment (Figure 1F). Immunoblots with α-pS141 demonstrated that RIN4 pS141 accumulated above steady state as early as 10–15 min post-flg22 treatment. Steady-state RIN4 levels remained constant, as detected by α-T7 antibody (Figure 2C). The detection of RIN4 pS141 could be blocked by addition of the original RIN4 pS141 phosphopeptide to extracts before immunoblotting with α-pS141 (Figure 2D). A parallel α-pS141 blot of the same extracts in the absence of competing phosphopeptide confirmed that flg22-induced RIN4 pS141 accumulation by 15 min posttreatment (Figure 2D). We also confirmed flg22-induced accumulation of RIN4 pS141 by immunoprecipitating total RIN4 with α-T7 and subsequently detecting either RIN4 pS141 (α-pS141) or total steady-state RIN4 (α-T7) by immunoblot. We noted the absence of detectable RIN4 pS141 in immunoprecipitates from transgenic plants expressing RIN4 S141A (Figure 2E). This result also defined a basal level of RIN4 pS141. We observed that flg22-induced RIN4 pS141 is

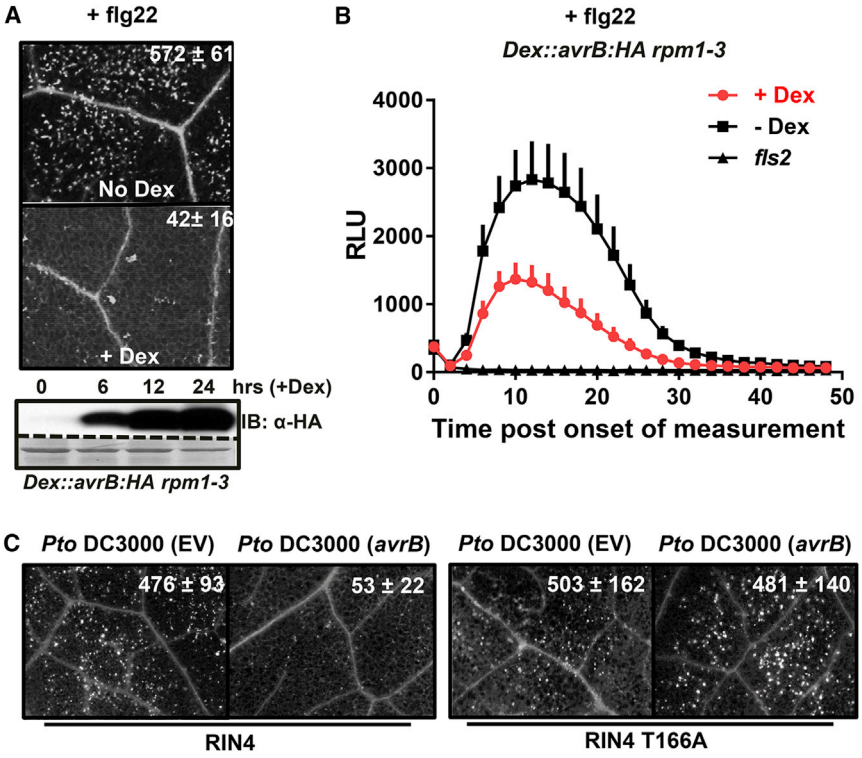

Figure 3. The T3E Protein AvrB Represses MTI via RIN4 T166

(A) Callose accumulation is reduced in transgenic *rpm1* plants conditionally expressing AvrB (*Dex::avrB:HA rpm1-3*). AvrB expression was induced by spraying 20 μM dexamethasone (Dex) 24 hr prior to treatment with 1 μM flg22. flg22-induced callose deposits were counted 18 hr after treatment (top and middle). Dex-induced AvrB accumulation was confirmed over time by immunoblot with α-HA (bottom). Callose deposit counts represent means and 2 × SE (n = 12); one of three independent experiments with similar results is shown.

(B) ROS burst in *Dex::avrB:HA rpm1-3* and *fls2* plants. Plants were pretreated with 20 μM Dex 24 hr prior to addition of 100 nM flg22-treatment and Luminol assay as in Figure 1D. Mock-treated *Dex::avrB:HA rpm1-3* plants were used as a control. Data were collected from 12 individual leaf discs (n = 12) for each genotype with four independent replicates. Error bars represent 2 × SE.

(C) AvrB suppression of callose accumulation requires RIN4 T166. Leaves of 5-week-old transgenic *rpm1 rps2 rin4* plants expressing either T7-tagged wild-type RIN4 (left panel) or RIN4 T166A (right panel) were inoculated with *Pto* DC3000 carrying either an empty vector (EV) or an isogenic *avrB* plasmid at 5 × 10^7 cfu/ml. Enhanced callose deposition was assayed 18 hr postinoculation. Data represent mean with 2 × SE (n = 20); one of three independent experiments with similar results is shown.

FLS2 dependent, consistent with this event being downstream of FLS2 activation during MTI (Figure 2F). Overexpression of RIN4 suppresses MTI outputs (Figure S3A) (Kim et al., 2005). We monitored flg22-induced RIN4 S141 phosphorylation in Col-0 and in transgenic Col-0 overexpressing RIN4 (OxRIN4), reasoning that excess RIN4 lacking phosphorylation of S141 might suppress MTI, since RIN4 S141A suppressed MTI outputs (Figure 1). Both Col-0 and OxRIN4 plants displayed similar amounts of pS141 upon flg22 treatment, despite their disparate overall RIN4 expression levels. We conclude that the ratio between pS141 and unphosphorylated RIN4 S141 is critical to enhance or suppress the MTI response (Figure 2G). This result is also consistent with enhanced MTI outputs in RIN4 S141E (Figure 1).

The data in Figure 2 collectively show that our α-pS141 reagent is specific, that resting state RIN4 contains low levels of RIN4 pS141, and that phosphorylation of S141 occurs rapidly following perception of flg22 and is dependent on FLS2 and abrogated in our RIN4 S141A mutant. Thus, we demonstrate a tight correlation between flg22 perception and selective phosphorylation of RIN4 S141 to derepress various MTI outputs. Consistent with this, we confirmed a previous observation (Qi et al., 2011) of coimmunoprecipitation of FLS2 with resting state RIN4 in planta (Figure S3B). Additionally, we observed that the elf18 peptide MAMP also induced accumulation of RIN4 pS141 (Figure S3C). These data suggest FLS2, or a kinase genetically downstream and potentially activated in complex with it (and perhaps also with the EFR1 receptor), are responsible for flg22-mediated accumulation of RIN4 pS141.

The T3E Protein AvrB Represses MTI via Enhancement of RIN4 T166 Phosphorylation

The precise mechanism by which any effector modulates RIN4 function as a negative regulator of MTI is not known. AvrB enhances RIPK-dependent accumulation of RIN4 pT166, and RPM1 is activated by increases in RIN4 pT166 levels (Chung et al., 2011; Liu et al., 2011). These studies suggested that AvrB contributes to pathogen virulence via enhancing phosphorylation on RIN4 T166 and consequent suppression of MTI but could not describe how because they were performed in plant genotypes that expressed RPM1 and RPS2.

We first addressed whether AvrB expression could suppress two of the flg22-driven MTI proxy outputs: callose deposition and ROS burst. We used transgenic *rpm1* plants to conditionally express AvrB following application of dexamethasone (Dex). Twenty-four hours after Dex application, we treated leaves with flg22 and assessed callose deposits 18 hr later. Mock-treated plants supported robust flg22-induced callose accumulation, while AvrB-expressing (Dex-treated) plants strongly suppressed this response (Figure 3A). Additionally, flg22-induced ROS burst was repressed in Dex-treated AvrB-expressing plants (Figure 3B). We also infiltrated leaves of transgenic *rpm1 rps2 rin4* plants expressing either wild-type RIN4 or RIN4 T166A with either *Pto* DC3000 or the same pathogen delivering native levels of AvrB via type III secretion (Figure 3C). Pathogen-induced callose deposition in transgenic plants expressing wild-type RIN4 was diminished following infiltration of AvrB-expressing bacteria (Figure 3C, left). This AvrB-mediated suppression was lost in transgenic plants expressing RIN4 T166A (Figure 3C, right).

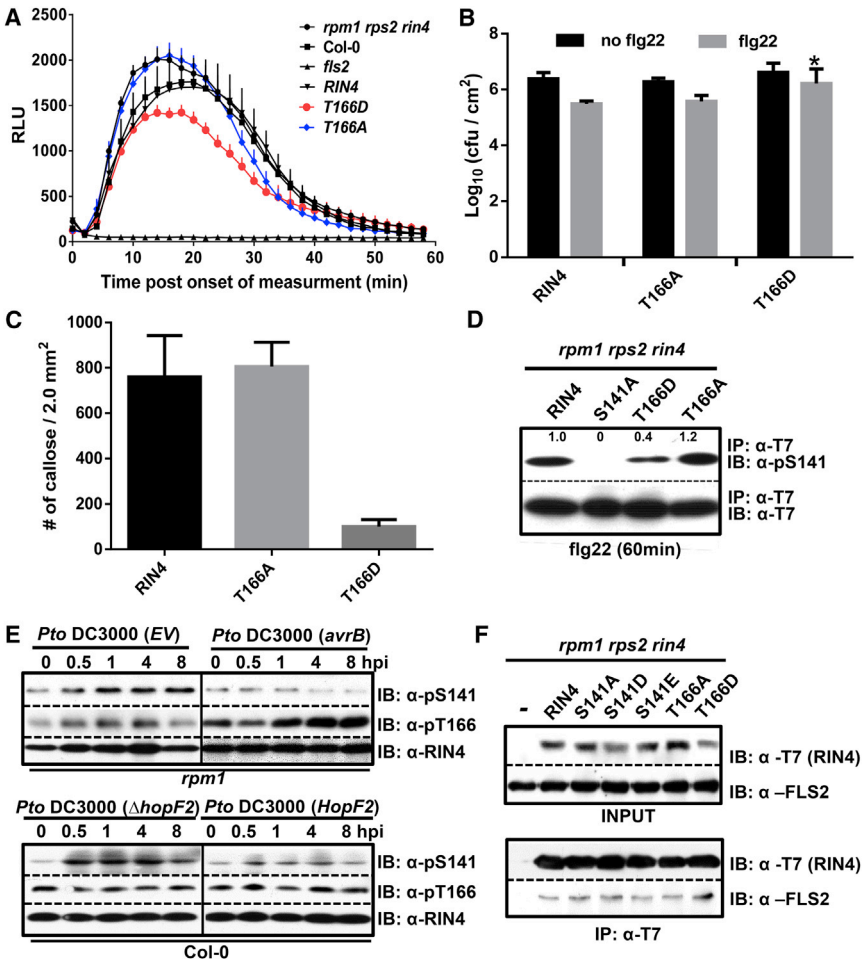

Figure 4. AvrB-Mediated Enhancement of RIN4 T166 Phosphorylation Suppresses RIN4 S141 Phosphorylation

(A) ROS burst in Col-0, *fls2*, *rpm1 rps2 rin4*, and *rpm1 rps2 rin4* plants expressing T7-tagged wild-type RIN4, RIN4 T166A, or RIN4 T166D. Luminol assays were performed as in Figure 1 after 100 nM flg22-treatment. Data were collected from 12 leaf discs (n = 12) for each genotype with four independent replicates. Error bars represent 2 × SE.

(B) Phosphomimic RIN4 T166D blocks flg22-activated bacterial growth suppression. Leaves of 5-week-old transgenic *rpm1 rps2 rin4* plants expressing T7-tagged wild-type RIN4, RIN4 T166A, or RIN4 T166D were preinoculated with 100 nM of flg22 (gray bars) or water (black bars). *Pto* DC3000(EV) bacteria were hand infiltrated at 1×10^5 cfu/ml 24 hr post flg22-treatment. Leaves were harvested for enumeration of bacteria 3 days later. The asterisk (*) denotes a significant difference compared to wild-type RIN4 determined by one-way ANOVA test followed by Tukey-Kramer HSD at 95% confidence.

(C) Phosphomimic RIN4 T166D blocks flg22 activated callose deposition. Leaves of 5-week-old transgenic *rpm1 rps2 rin4* plants expressing T7-tagged wild-type RIN4, RIN4 T166A, or RIN4 T166D were infiltrated with 1 μM flg22 and monitored for induced callose accumulation 18 hr later. Callose deposit counts represent means with 2 × SE (n = 16 per genotype).

(D) Expression of RIN4 T166D dampens flg22-dependent phosphorylation of RIN4 S141. Transgenic *rpm1 rps2 rin4* plants expressing T7-tagged wild-type RIN4, RIN4 S141A, RIN4 T166D, or RIN4 T166A were inoculated with 1 μM flg22. Leaves were harvested 60 min postelicitation. Immunoblot of total extracts with α-pS141 was performed after immunoprecipitiation with α-T7. Equal loading was confirmed by α-T7 blot. Numbers in the α-pS141 blot lanes represent the relative expression levels of RIN4 pS141 normalized to the respective α-T7 immunoblot.

(E) Phosphorylation of RIN4 S141 and T166 in response to AvrB or HopF2 delivered from bacteria. *Pto* DC3000(EV) and *Pto* DC3000(*avrB*) (top) or *Pto* DC3000(*ΔhopF2*) and *Pto* DC3000(*HopF2*^{ATG}) (bottom) were infiltrated at 5×10^7 cfu/ml into leaves of *rpm1-3* or Col-0 plants. Tissue samples were collected at the indicated hours postinfection. Immunoblots of total extracts were performed with either α-pS141 or α-pT166. Similar results were obtained from two independent experiments. Loading was confirmed by immunoblot with α-RIN4.

(F) Coimmunoprecipitation of FLS2 with resting state RIN4-, S141-, and T166-derived mutants. Transgenic *rpm1 rps2 rin4* plants expressing T7-RIN4 or mutants were used for immunoprecipitation with α-T7. Coimmunoprecipitated FLS2 was detected by immunoblot with α-FLS2. Similar results were observed in two independent replicates.

We previously defined AvrB residues that did not compromise type III secretion into plant cells but were required for activation of RPM1. Some of these retained the ability to interact with RIN4 (Desveaux et al., 2007). If the same function of AvrB that triggers RPM1 activity, namely the enhanced accumulation of RIN4 pT166, is required for its virulence function, we predicted that AvrB mutants unable to activate RPM1 would also lose the ability to suppress callose deposition. We repeated our pathogen-induced callose deposition assays using *Pto* DC3000 carrying wild-type *avrB* or mutant loss of function alleles *avrB G2A*, *avrB Y65A, avrB T125A*, and *avrB D297A.* AvrB mutants that cannot activate RPM1 also did not suppress pathogen-induced callose deposition, although they accumulated equally (Figure S4). These data are consistent with a model where AvrB-enhanced, RIPK-dependent accumulation of RIN4 pT166 suppresses at least these MTI outputs in *rpm1* plants.

AvrB-Mediated Enhancement of RIN4 T166 Phosphorylation Suppresses RIN4 S141 Phosphorylation

We also generated transgenic plants expressing RIN4 T166D from the native promoter to address whether the phospho-status of RIN4 T166 can modulate flg22-dependent responses that require RIN4 pS141. We monitored MTI outputs following flg22-treatment using these transgenic lines and isogenic lines expressing wild-type RIN4; wild-type Col-0, *fls2* and the parental *rpm1 rps2 rin4* line served as controls. The slight but obviously enhanced and more rapid flg22-dependent ROS burst observed in the parental *rpm1 rps2 rin4* line was maintained in plants expressing RIN4 T166A and complemented back to Col-0 levels by expression of wild-type RIN4. Expression of the RIN4 T166D phosphomimic significantly suppressed flg22-dependent ROS burst (Figure 4A), similar to what we observed in Dex-treated *Dex::AvrB rpm1* plants (Figure 3B). The flg22-activated

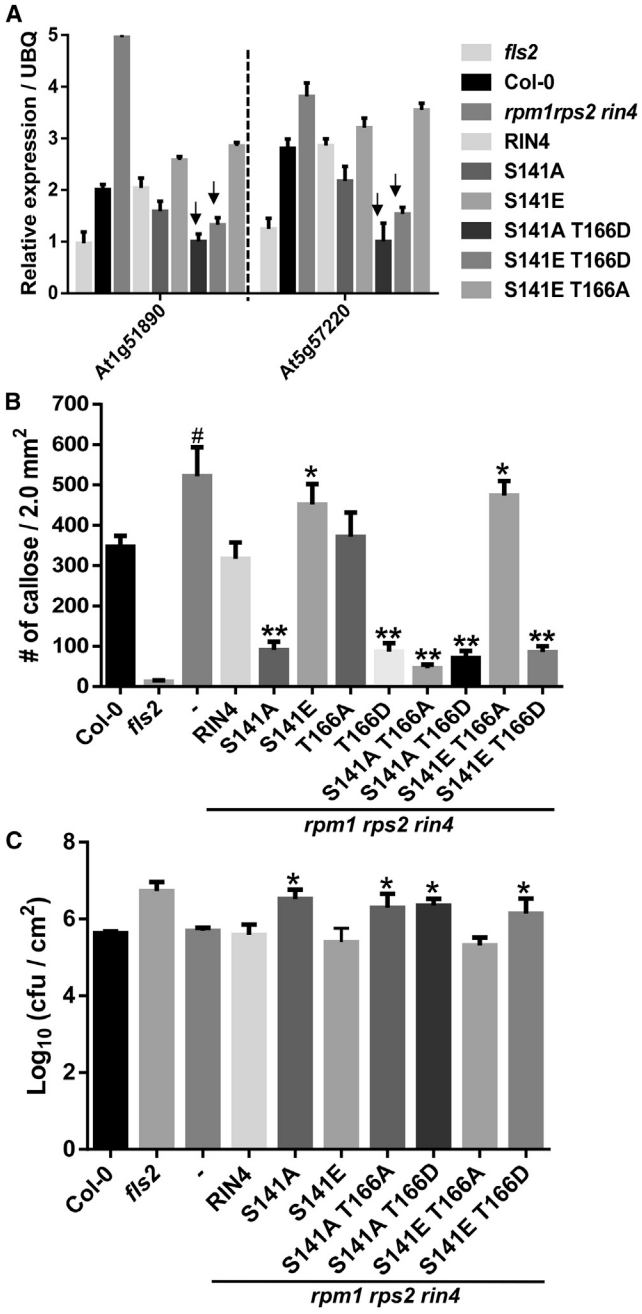

Figure 5. RIN4 T166 Phosphorylation Is Epistatic to pRIN4 S141

(A) Early defense gene expression in response to 1μM flg22 in leaves of transgenic *rpm1 rps2 rin4* plants expressing T7-tagged RIN4 derivatives as noted. Quantitative PCR was performed as Figure 1F. Arrowheads highlight the reduction of induced defense gene expression in plants expressing RIN4 T166D. Error bars represent 2 × SE (n = 3); the experiment was performed two times.

(B) Callose accumulation in transgenic *rpm1 rps2 rin4* plants expressing T7-tagged RIN4 derivatives as noted. Number of callose deposits was monitored as Figure 1. Data demonstrate mean with 2 × SE (n = 18); the experiment was performed two times. Number (#) sign denotes significant difference compared to Col-0 using one-way ANOVA test with Tukey-Kramer HSD with 95% confidence. Asterisks (* or **) demonstrate significant differences compared to RIN4 using one-way ANOVA test with Tukey-Kramer HSD with 95% confidence.

(C) flg22-activated bacterial growth suppression in transgenic *rpm1 rps2 rin4* plants expressing T7-tagged RIN4 derivatives as noted. Three independent experiments were performed as Figure 1. Asterisks (*) denote significant differences compared to wild-type RIN4 by one-way ANOVA test with Tukey-Kramer HSD with 95% confidence. For graphical clarity, data displayed here in (B) and (C) are derived from the same experiments shown in Figures S6B and S6C, respectively. The only difference is the exchange of data from transgenic lines expressing RIN4 S141E singly and in combinations (here) with data of transgenic lines expressing RIN4 S141D (Figure S6).

suppression of *Pto* DC3000 proliferation was retained in plants expressing wild-type RIN4 or RIN4 T166A but was lost in plants expressing the RIN4 T166D phosphomimic (Figure 4B). Plants expressing RIN4 T166D were unable to support full flg22-mediated, RIN4 pS141-dependent callose deposition (Figures 4C and S5). These observations strongly suggest that the RIN4 T166D phosphomimic antagonizes the phosphorylation of RIN4 S141 that, as detailed above, contributes to several MTI output responses. We tested this directly by determining the level of flg22-induced pS141 in immunoprecipitates of plants expressing RIN4 T166A or RIN4 T166D. We noted that there was ~2- to 3-fold less pS141 on RIN4 T166D molecules than on wild-type or RIN4 T166A molecules (Figure 4D). Finally, we confirmed that RIN4 pS141 is induced in wild-type Col-0 plants inoculated with pathogenic *Pto* DC3000 but that inoculation of *Pto* DC3000(*avrB*) preferentially induces accumulation of RIN4 pT166. Notably, this event correlates strongly with the absence of RIN4 pS141 accumulation (Figure 4E, top). Delivery of HopF2 inhibited RIN4 pS141 accumulation in the absence of increased RIN4 pT166 (Figure 4E, bottom). While HopF2 targets RIN4 (Wilton et al., 2010), it also targets the FLS2 coreceptor BAK1 and the BIK1 RLCK that acts downstream of FLS2 (Wang et al., 2010; Zhou et al., 2014). Thus, our result likely represents the cumulative effects of HopF2 on RIN4 and these upstream kinases. Nevertheless, multiple effector biochemical mechanisms on RIN4 result in diminution of RIN4 pS141 and thus favor rerepression of MTI. Interestingly, we found that similar amounts of RIN4 can associate with FLS2 regardless of phosphorylation status on either S141 or T166 (Figure 4F).

RIN4 T166 Phosphorylation Is Epistatic to pRIN4 S141

The time course of specific phosphorylation shown in Figure 4E suggested that AvrB-dependent enhancement of RIN4 pT166 blocks or dampens MAMP-driven phosphorylation of RIN4 S141. To test this, we generated transgenic plants expressing comparable levels of RIN4 *cis* double mutations in S141 and T166 in the *rpm1 rps2 rin4* triple mutant background (Figure S6A). We again examined several MTI outputs: early defense gene expression, flg22-induced resistance to pathogenic bacteria, and flg22-induced callose accumulation (Figure 5). Flg22-induced defense gene expression was enhanced in RIN4 S141E and RIN4 S141E T166A compared to wild-type RIN4 (Figure 5A). In contrast, plants expressing RIN4 T166D-containing mutants, especially RIN4 S141E T166D, exhibited marker gene expression reduced to levels matching the *fls2* mutant (Figure 5A, arrows). We measured flg22-induced callose accumulation and noted that plants expressing RIN4 S141E and RIN4 S141E T166A *cis* double mutations exhibited enhanced callose deposition, approximating that of the *rin4*-null parent line, compared to

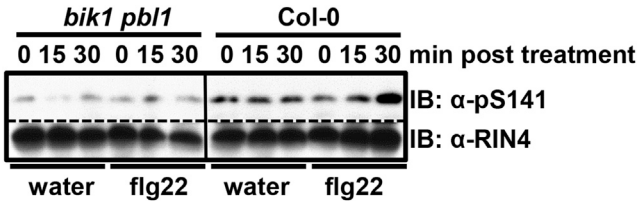

Figure 6. Genetic Requirement of RIN4 S141 Phosphorylation upon MTI Activation

Five-week-old Col-0 and *bik1 pbl1* double mutant plants were used to monitor induced RIN4 pS141 at 0, 15, and 30 min post-flg22 treatment. Mock treatment on the same plants were used as negative control for induced pS141. Similar result was observed in two independent repeats.

Col-0 and plants expressing wild-type RIN4 (Figure 5B, columns 6 and 11). In contrast, plants expressing RIN4 T166D-containing derivatives, in particular RIN4 S141E T166D, were unable to support flg22-induced callose depositions compared to Col-0 and plants expressing wild-type RIN4 (Figure 5B, columns 8, 10, and 12). We monitored flg22-induced bacterial growth suppression and observed that plants expressing RIN4 S141E and RIN4 S141E T166A *cis* double mutations restricted bacterial growth, as did Col-0 and wild-type RIN4 (Figure 5C, columns 6 and 9). In contrast, plants expressing RIN4 T166D-containing derivatives, in particular RIN4 S141E T166D, were unable to restrict bacterial pathogen proliferation (Figure 5C, columns 8 and 10). Notably, plants expressing RIN4 S141A in any combination were unable to suppress callose deposition or restrict pathogen growth (Figures 5B and 5C). We confirmed the sum of these results using independent transgenic lines expressing the alternative RIN4 S141D phosphomimic (Figures S6B and S6C). Hence, the phosphomimic RIN4 T166D is epistatic to all MTI outputs that are enhanced by the phosphomimic RIN4 S141E/D. Together, data in Figures 4 and 5 support our contention that AvrB interaction with RIN4 and consequent enhancement of RIN4 pT166 levels overrides the MAMP-induced accumulation of RIN4 pS141 required to derepress MTI signaling.

RLCKs Are Required for RIN4 pS141 Accumulation upon MTI Activation

The RLCK BIK1 plays a key role in the transduction of signals from activated PRRs (Lu et al., 2010; Li et al., 2014). A BIK1 paralog, PBS-like 1 (PBL1) also contributes to PRR-dependent MTI additively with BIK1 (Zhang et al., 2010). We compared flg22-dependent RIN4 pS141 accumulation in *bik1 pbl1* to that in Col-0. We observed decreased basal RIN4 pS141 levels in *bik1 pbl1* compared to Col-0, suggesting that BIK1 and/or PBL1 are required for maintaining basal levels of RIN4 pS141. Moreover, flg22-induced RIN4 S141 phosphorylation was not observed in *bik1 pbl1* as it was in Col-0 (Figure 6), demonstrating that BIK1 and PBL1 are required for the regulated accumulation of RIN4 pS141.

DISCUSSION

The functional relevance of RIN4 in regulation of MTI is illustrated by the evolution of four different bacterial T3Es that perform at least three distinct biochemical modifications on it to regulate

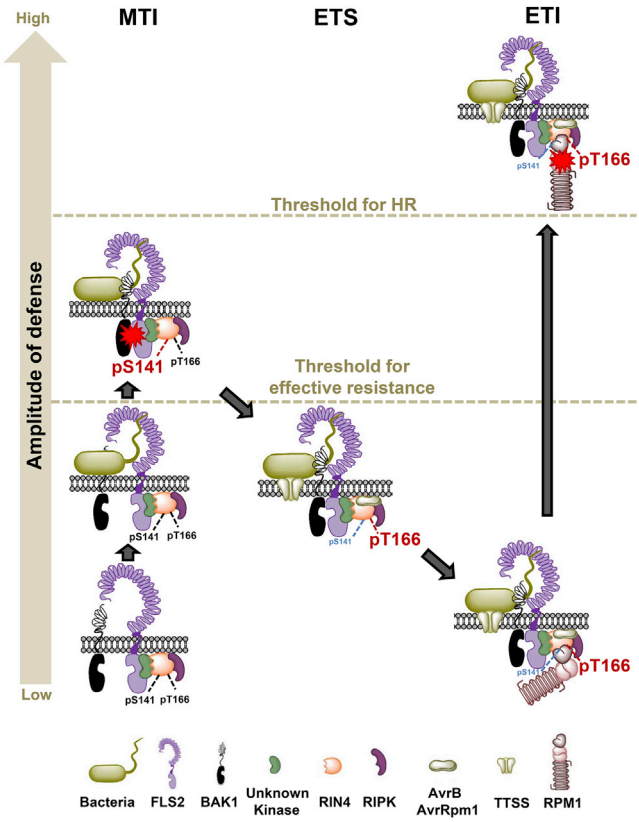

Figure 7. Model for a "Molecular-Switch" Function of RIN4 in MTI, ETS, and ETI

Activation of MTI. RIN4 associates with FLS2 and probably RIPK. Steady-state phosphorylation of RIN4 S141 and T166 maintains the resting state (left column, bottom). Following infection (left column, middle), flg22 perception through FLS2 induces RIN4 phosphorylation on S141 via an unknown kinase(s). Increased RIN4 pS141 contributes to derepression of MTI outputs above a signal threshold (left column, top).

Bacterial T3E proteins repress MTI to induce ETS. Activation of type III gene expression and delivery of AvrB and AvrRpm1 antagonize MAMP-induced (here flg22) accumulation of RIN4 pS141 by enhancing RIPK-mediated accumulation of RIN4 pT166, rerepressing MTI below the signaling threshold to establish ETS (middle column).

Enhanced ETI. The *Arabidopsis* RPM1 NLR receptor has evolved (right column, bottom) to associate with steady-state RIN4 and is activated by the overaccumulation of RIN4 pT166 to turn on ETI (right column, top).

plant immune system function. Additionally, two intracellular *Arabidopsis* NLR immune receptors, RPM1 and RPS2 associate with RIN4, and are activated by different effector-mediated alterations of it. Genomes for all land plants sequenced to date encode RIN4 orthologs (see Introduction; Figure S1E). Our data support an evolutionarily generalizable model wherein the balance between RIN4 pT166 (MTI off) and RIN4 pS141 (MTI on) regulates RIN4 contributions to MTI. This model further explains how plant evolution has responded by deploying various NLR receptors to sense effector-mediated manipulation of RIN4 (Figure 7).

An equilibrated basal phosphorylation of S141 and T166 residues maintains a RIN4 resting state that negatively regulates MTI (Figure 7, lower left). Upon infection, PRRs like

FLS2 or EFR are activated; this induces enhanced RIN4 pS141 accumulation to derepress MTI; this event requires BIK1 and/or PBL1 (Figure 7, upper left). RIN4 S141 is required for some MTI outputs and contributes quantitatively to others, and RIN4 S141 phosphomimic alleles express enhanced MTI outputs. Redundancy of RIN4 paralogs might also contribute to MTI; these can share residues equivalent to RIN4 T166 (Chung et al., 2011). This flg22-driven accumulation of RIN4 pS141 is FLS2 dependent; native levels of FLS2 and RIN4 can be coimmunoprecipitated at resting steady state, and all of the examined RIN4 phospho mutants retain association with FLS2 in planta. Thus, we suggest that RIN4 is a component of the FLS2 immune complex independent of its S141 phosphorylation status (Macho and Zipfel, 2014). Binding of flg22 by FLS2 drives heteromerization with BAK1 (Sun et al., 2013). BAK1 also plays a key role in activation of MTI upon recognition of elf18 by EFR. The FLS2-BAK1 immune complex contains BIK1, which positively regulates MTI via trans-phosphorylation of FLS2 and BAK1, disassociates from the receptor complex, and phosphorylates several targets (Macho and Zipfel, 2014). Our results indicate that both FLS2- and EFR-dependent MTI responses share RIN4 S141 as a common downstream target. Thus, we speculate that BIK1 and/or PBL1 act either directly on RIN4 or act through a functionally overlapping, related RLCK to phosphorylate RIN4 S141 upon PRR activation to derepress MTI. We are currently pursuing this speculation experimentally.

Type III secretion system genes begin expression after infection and delivery of AvrB blocks accumulation of RIN4 pS141 by enhancing RIPK activity on RIN4 pT166 (Figure 7, middle and top). RIPK expression is rapidly and specifically upregulated upon RPM1 activation; this would reinforce enhanced accumulation of RIN4 pT166 (Liu et al., 2011). Thus, in naturally occurring plant genotypes that lack *RPM1* (Rose et al., 2012), AvrB and AvrRpm1 contribute to ETS via suppression of MTI (Ashfield et al., 2004; Ritter and Dangl, 1995) (Figure 6, middle). AvrB does so by enhancing RIPK activity to re-establish a relatively high ratio of RIN4 pT166 to RIN4 pS141 and thus facilitates rerepression of MTI; AvrRpm1 also does so at least in part via RIPK (Chung et al., 2011; Liu et al., 2011). Importantly, we demonstrated that the RIN4 T166D phosphomimic (which rerepresses RIN4 contributions to MTI) is fully epistatic to RIN4 S141E (which derepresses RIN4 contributions to MTI). This is consistent with a temporal requirement for AvrB-mediated virulence function in the face of ongoing MTI responses generated via RIN4 pS141.

The NLR receptor RPM1, when present, is activated by AvrB (and AvrRpm1) modulation of RIN4 pT166 levels (Figure 7, right) (Chung et al., 2011; Liu et al., 2011), leading to high amplitude ETI. The NLRs in soybean that are activated by AvrB or AvrRpm1, or both, are also responding to manipulation of the steady-state levels of the phosphorylated threonine at the position orthologous to RIN4 T166 in soybean (Selote et al., 2012). A knife's edge balance of resting state RIN4 pT166 sufficient to maintain repression of MTI while avoiding ectopic RPM1 activation likely explains the demonstrated fitness cost of RPM1 (Tian et al., 2003). This model sets the stage for biochemical characterization of the relevant kinase complexes over the time course from resting state through activation of MTI, effector-mediated rerepression of RIN4 function, and the consequent activation of RIN4-associated NLR sensor receptors.

EXPERIMENTAL PROCEDURES

Vector Construction

See Supplemental Experimental Procedures.

Plants

Standard methods were employed. See Supplemental Experimental Procedures.

ROS Burst

Twelve leaf discs from 4-week-old Col-0, *fls2, rpm1 rps2 rin4*, and transgenic plants expressing RIN4 wild-type or RIN4 mutants were placed into 12 wells of a 96-well plate with 150 μl of water in each well. After overnight incubation, 100 μl of reaction mix, including 17 μg/ml of Luminol (Sigma), 10 μg/ml of Horseradish Peroxidase (HRP; Sigma), and 100 nM flg22, was substituted for the water to monitor ROS burst (Boutrot et al., 2010; Roux et al., 2011). Luminescence was measured immediately with 1 s integration and 2 min interval over 60 min by using a SpectraMax L (Molecular Device).

MAP Kinase Activation

MAPK activation was monitored on 4-week-old *Arabidopsis* plants. Leaf samples were collected 0, 10, 20, and 30 min post-100 nM flg22 treatment by hand infiltration and frozen in liquid nitrogen (Roux et al., 2011). Immunoblot with anti-phospho-p44/42 MAPK (Erk1/2) (Thr202/Tyr204) rabbit monoclonal antibodies (Cell Signaling) was used to monitor induced MAPK activation. Coomassie brilliant blue staining of RuBisCo was used as loading control.

Quantitative RT-PCR

RNA samples were quantified with a Nanodrop spectrophotometer (Thermo Scientific; Hudson). First-strand cDNA was synthesized from 1 μg RNA using SuperScript RNA H- Reverse Transcriptase (Invitrogen; Grand Island) and an oligo (dT) primer following manufacturer's instructions. Triplicate samples of cDNA were amplified by quantitative PCR using SYBR Green (Sigma Aldrich; Saint Louis) and the ViiA 7 (Applied Biosystems; Grand Island). The relative expression values were determined using *UBQ10* as a reference by the comparative Ct method (2-ΔΔCt) according to the manufacturer's protocol (Applied Biosystems; Grand Island).

Callose Assay

Five-week-old *Arabidopsis* plants were infiltrated with 1 μM of flg22 on the lower leaf surface (Boutrot et al., 2010). To visualize callose deposition, leaves were stained with aniline blue (Kim et al., 2005). In brief, the tissue was cleared and dehydrated with 100% EtOH overnight at 37°C. Cleared leaves were washed with distilled water and then stained in 0.01% aniline blue in 150 mM K_2HPO_4 (pH 9.5) for 4 hr at room temperature. Stained samples were washed and mounted in distilled water and examined by epifluorescence (LEICA M205 FA) with 100× magnification. Images were taken at the region below the infiltrated zone of each leaf. Counting of accumulated callose foci was carried out using ImageJ (NIH).

Measurement of ROS Burst

The flg22 peptide (QRLSTGSRINSAKDDAAGLQIA) was synthesized according to the conserved N-terminal region of eubacterial flagellin (Genscript) (Felix et al., 1999; Zipfel et al., 2004). ROS burst was measured as in Supplemental Experimental Procedures.

Bacterial Growth Suppression Assay

Water or 100 nM flg22 (Boutrot et al., 2010) was infiltrated with a needleless syringe into leaves of 5-week-old *Arabidopsis* plants. A solution of 1×10^5 cfu/ml of *Pto* DC3000 bacteria were syringe-infiltrated 24 hr later. Bacterial growth was determined 3 days postinoculation.

Protein Extraction, Immunoblot, and Coimmunoprecipitation Analyses

See Supplemental Experimental Procedures.

Quantification of Hypersensitive Response In planta

See Supplemental Experimental Procedures.

Statistical Analysis

Statistical significance was based on one-way ANOVA analyses performed with JMP10.0 software (SAS).

SUPPLEMENTAL INFORMATION

Supplemental Information includes six figures, one table, and Supplemental Experimental Procedures and can be found with this article online at http://dx.doi.org/10.1016/j.chom.2014.09.004.

AUTHOR CONTRIBUTIONS

E.-H.C. and J.L.D. designed experiments. E.-H.C., F.E.-K., Y. H., and A.L. performed experiments. E.-H.C., F.E.-K., and J.L.D. wrote the paper.

ACKNOWLEDGMENTS

We thank Drs. Sarah Grant, Marc Nishimura, Petra Epple, and Ryan Anderson for critical comments on the manuscript and all of the Dangl-Grant lab members for fruitful discussions. We thank Dr. Cyril Zipfel, Sainsbury Lab, Norwich, for the gift of anti-FLS2 sera sera and *bik1 pbl1* double mutant seed. F.E.-K. is a recipient of a German Research Society (DFG) Postdoctoral fellowship (EL 734/1-1). Y.H. was supported by a Distinguished Guest Professorship, Eberhard-Karls-Universität, Tübingen, Germany to J.L.D. This work was funded by grants to J.L.D. from the National Science Foundation IOS-0929410 (Arabidopsis 2010 Program) and IOS-1257373 and by the HHMI and the Gordon and Betty Moore Foundation (GBMF3030). J.L.D. is an Investigator of the Howard Hughes Medical Institute.

Received: May 21, 2014
Revised: August 7, 2014
Accepted: August 29, 2014
Published: October 8, 2014

REFERENCES

Ashfield, T., Ong, L.E., Nobuta, K., Schneider, C.M., and Innes, R.W. (2004). Convergent evolution of disease resistance gene specificity in two flowering plant families. Plant Cell *16*, 309–318.

Axtell, M.J., and Staskawicz, B.J. (2003). Initiation of RPS2-specified disease resistance in Arabidopsis is coupled to the AvrRpt2-directed elimination of RIN4. Cell *112*, 369–377.

Belkhadir, Y., Yang, L., Hetzel, J., Dangl, J.L., and Chory, J. (2014). The growth-defense pivot: crisis management in plants mediated by LRR-RK surface receptors. Trends Biochem. Sci. http://dx.doi.org/10.1016/j.tibs.2014.06.006.

Benschop, J.J., Mohammed, S., O'Flaherty, M., Heck, A.J., Slijper, M., and Menke, F.L. (2007). Quantitative phosphoproteomics of early elicitor signaling in Arabidopsis. Mol. Cell. Proteomics *6*, 1198–1214.

Boutrot, F., Segonzac, C., Chang, K.N., Qiao, H., Ecker, J.R., Zipfel, C., and Rathjen, J.P. (2010). Direct transcriptional control of the Arabidopsis immune receptor FLS2 by the ethylene-dependent transcription factors EIN3 and EIL1. Proc. Natl. Acad. Sci. USA *107*, 14502–14507.

Chinchilla, D., Zipfel, C., Robatzek, S., Kemmerling, B., Nürnberger, T., Jones, J.D., Felix, G., and Boller, T. (2007). A flagellin-induced complex of the receptor FLS2 and BAK1 initiates plant defence. Nature *448*, 497–500.

Chung, E.H., da Cunha, L., Wu, A.J., Gao, Z., Cherkis, K., Afzal, A.J., Mackey, D., and Dangl, J.L. (2011). Specific threonine phosphorylation of a host target by two unrelated type III effectors activates a host innate immune receptor in plants. Cell Host Microbe *9*, 125–136.

Coaker, G., Falick, A., and Staskawicz, B. (2005). Activation of a phytopathogenic bacterial effector protein by a eukaryotic cyclophilin. Science *308*, 548–550.

Desveaux, D., Singer, A.U., Wu, A.J., McNulty, B.C., Musselwhite, L., Nimchuk, Z., Sondek, J., and Dangl, J.L. (2007). Type III effector activation via nucleotide binding, phosphorylation, and host target interaction. PLoS Pathog. *3*, e48.

Dodds, P.N., and Rathjen, J.P. (2010). Plant immunity: towards an integrated view of plant-pathogen interactions. Nat. Rev. Genet. *11*, 539–548.

Felix, G., Duran, J.D., Volko, S., and Boller, T. (1999). Plants have a sensitive perception system for the most conserved domain of bacterial flagellin. Plant J. *18*, 265–276.

Feng, F., and Zhou, J.M. (2012). Plant-bacterial pathogen interactions mediated by type III effectors. Curr. Opin. Plant Biol. *15*, 469–476.

Feng, F., Yang, F., Rong, W., Wu, X., Zhang, J., Chen, S., He, C., and Zhou, J.M. (2012). A Xanthomonas uridine 5′-monophosphate transferase inhibits plant immune kinases. Nature *485*, 114–118.

Grant, M., Brown, I., Adams, S., Knight, M., Ainslie, A., and Mansfield, J. (2000). The RPM1 plant disease resistance gene facilitates a rapid and sustained increase in cytosolic calcium that is necessary for the oxidative burst and hypersensitive cell death. Plant J. *23*, 441–450.

Huynh, T.V., Dahlbeck, D., and Staskawicz, B.J. (1989). Bacterial blight of soybean: regulation of a pathogen gene determining host cultivar specificity. Science *245*, 1374–1377.

Jones, J.D., and Dangl, J.L. (2006). The plant immune system. Nature *444*, 323–329.

Kim, M.G., da Cunha, L., McFall, A.J., Belkhadir, Y., DebRoy, S., Dangl, J.L., and Mackey, D. (2005). Two *Pseudomonas syringae* type III effectors inhibit RIN4-regulated basal defense in Arabidopsis. Cell *121*, 749–759.

Li, L., Li, M., Yu, L., Zhou, Z., Liang, X., Liu, Z., Cai, G., Gao, L., Zhang, X., Wang, Y., et al. (2014). The FLS2-associated kinase BIK1 directly phosphorylates the NADPH oxidase RbohD to control plant immunity. Cell Host Microbe *15*, 329–338.

Liu, J., Elmore, J.M., Lin, Z.J., and Coaker, G. (2011). A receptor-like cytoplasmic kinase phosphorylates the host target RIN4, leading to the activation of a plant innate immune receptor. Cell Host Microbe *9*, 137–146.

Lu, D., Wu, S., Gao, X., Zhang, Y., Shan, L., and He, P. (2010). A receptor-like cytoplasmic kinase, BIK1, associates with a flagellin receptor complex to initiate plant innate immunity. Proc. Natl. Acad. Sci. USA *107*, 496–501.

Macho, A.P., and Zipfel, C. (2014). Plant PRRs and the activation of innate immune signaling. Mol. Cell *54*, 263–272.

Mackey, D., Holt, B.F., 3rd, Wiig, A., and Dangl, J.L. (2002). RIN4 interacts with *Pseudomonas syringae* type III effector molecules and is required for RPM1-mediated resistance in Arabidopsis. Cell *108*, 743–754.

Mackey, D., Belkhadir, Y., Alonso, J.M., Ecker, J.R., and Dangl, J.L. (2003). Arabidopsis RIN4 is a target of the type III virulence effector AvrRpt2 and modulates RPS2-mediated resistance. Cell *112*, 379–389.

Mukhtar, M.S., Carvunis, A.R., Dreze, M., Epple, P., Steinbrenner, J., Moore, J., Tasan, M., Galli, M., Hao, T., Nishimura, M.T., et al.; European Union Effectoromics Consortium (2011). Independently evolved virulence effectors converge onto hubs in a plant immune system network. Science *333*, 596–601.

Nimchuk, Z., Marois, E., Kjemtrup, S., Leister, R.T., Katagiri, F., and Dangl, J.L. (2000). Eukaryotic fatty acylation drives plasma membrane targeting and enhances function of several type III effector proteins from Pseudomonas syringae. Cell *101*, 353–363.

Nühse, T.S., Stensballe, A., Jensen, O.N., and Peck, S.C. (2004). Phosphoproteomics of the Arabidopsis plasma membrane and a new phosphorylation site database. Plant Cell *16*, 2394–2405.

Nühse, T.S., Bottrill, A.R., Jones, A.M., and Peck, S.C. (2007). Quantitative phosphoproteomic analysis of plasma membrane proteins reveals regulatory mechanisms of plant innate immune responses. Plant J. *51*, 931–940.

Qi, Y., Tsuda, K., Glazebrook, J., and Katagiri, F. (2011). Physical association of pattern-triggered immunity (PTI) and effector-triggered immunity (ETI) immune receptors in Arabidopsis. Mol. Plant Pathol. *12*, 702–708.

Ritter, C., and Dangl, J.L. (1995). The avrRpm1 gene of Pseudomonas syringae pv. maculicola is required for virulence on Arabidopsis. Mol. Plant Microbe Interact. *8*, 444–453.

Rose, L., Atwell, S., Grant, M., and Holub, E.B. (2012). Parallel Loss-of-Function at the RPM1 Bacterial Resistance Locus in Arabidopsis thaliana. Front. Plant Sci. *3*, 287.

Roux, M., Schwessinger, B., Albrecht, C., Chinchilla, D., Jones, A., Holton, N., Malinovsky, F.G., Tör, M., de Vries, S., and Zipfel, C. (2011). The Arabidopsis leucine-rich repeat receptor-like kinases BAK1/SERK3 and BKK1/SERK4 are required for innate immunity to hemibiotrophic and biotrophic pathogens. Plant Cell *23*, 2440–2455.

Schwessinger, B., Roux, M., Kadota, Y., Ntoukakis, V., Sklenar, J., Jones, A., and Zipfel, C. (2011). Phosphorylation-dependent differential regulation of plant growth, cell death, and innate immunity by the regulatory receptor-like kinase BAK1. PLoS Genet. *7*, e1002046.

Selote, D., Robin, G.P., and Kachroo, A. (2012). GmRIN4 protein family members function nonredundantly in soybean race-specific resistance against Pseudomonas syringae. New Phytol. *197*, 1225–1235.

Sun, Y., Li, L., Macho, A.P., Han, Z., Hu, Z., Zipfel, C., Zhou, J.M., and Chai, J. (2013). Structural basis for flg22-induced activation of the Arabidopsis FLS2-BAK1 immune complex. Science *342*, 624–628.

Tian, D., Traw, M.B., Chen, J.Q., Kreitman, M., and Bergelson, J. (2003). Fitness costs of R-gene-mediated resistance in Arabidopsis thaliana. Nature *423*, 74–77.

Wang, Y., Li, J., Hou, S., Wang, X., Li, Y., Ren, D., Chen, S., Tang, X., and Zhou, J.M. (2010). A Pseudomonas syringae ADP-ribosyltransferase inhibits Arabidopsis mitogen-activated protein kinase kinases. Plant Cell *22*, 2033–2044.

Wilton, M., Subramaniam, R., Elmore, J., Felsensteiner, C., Coaker, G., and Desveaux, D. (2010). The type III effector HopF2Pto targets Arabidopsis RIN4 protein to promote Pseudomonas syringae virulence. Proc. Natl. Acad. Sci. USA *107*, 2349–2354.

Zhang, J., Li, W., Xiang, T., Liu, Z., Laluk, K., Ding, X., Zou, Y., Gao, M., Zhang, X., Chen, S., et al. (2010). Receptor-like cytoplasmic kinases integrate signaling from multiple plant immune receptors and are targeted by a *Pseudomonas syringae* effector. Cell Host Microbe *7*, 290–301.

Zhou, J., Wu, S., Chen, X., Liu, C., Sheen, J., Shan, L., and He, P. (2014). The Pseudomonas syringae effector HopF2 suppresses Arabidopsis immunity by targeting BAK1. Plant J. *77*, 235–245.

Zipfel, C., Robatzek, S., Navarro, L., Oakeley, E.J., Jones, J.D., Felix, G., and Boller, T. (2004). Bacterial disease resistance in Arabidopsis through flagellin perception. Nature *428*, 764–767.

Cell Host & Microbe, Volume *16*

Supplemental Information

A Plant Phosphoswitch Platform Repeatedly Targeted by Type III Effector Proteins Regulates the Output of Both Tiers of Plant Immune Receptors

Eui-Hwan Chung, Farid El-Kasmi, Yijian He, Alex Loehr, and Jeffery L. Dangl

SUPPLEMENTAL FIGURES

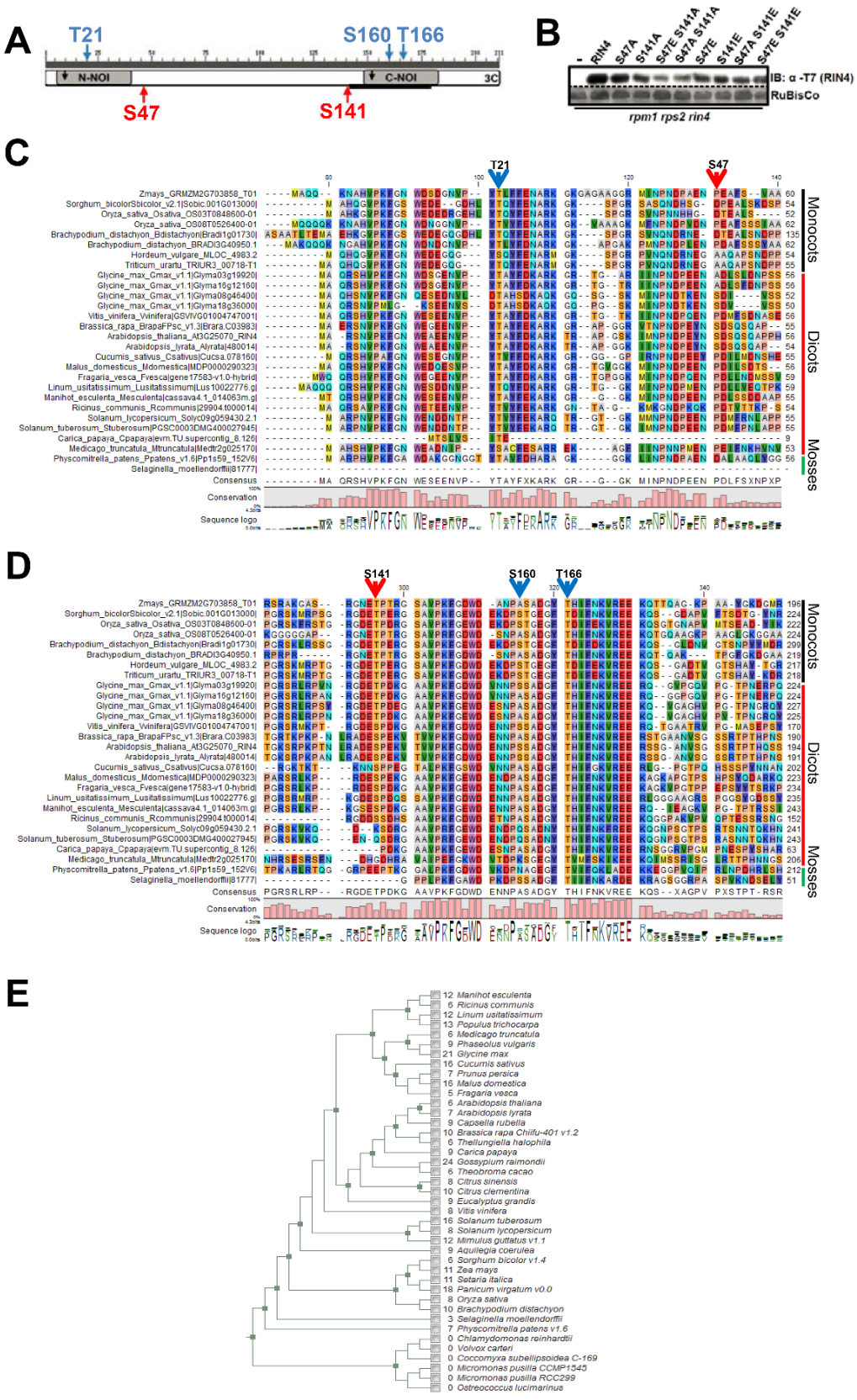

Figure S1, related to Figure1. RIN4 phosphorylation sites and conservation in land plants and the expression levels of RIN4 mutant alleles.

(A) Schematic diagram positioning the putative phosphorylated residues of RIN4. Threonine 21, serine 160 and threonine 166 residues are phosphorylated by RPM1-inducing protein kinase (RIPK) (blue down arrows). Phosphorylation of serine 47 and serine 141 residue is induced during MAMP-triggered immunity (MTI; red up arrows). Gray boxes indicate RIN4 N and C-terminal NOI domains. The AvrB binding site is indicated by a black bar. Black arrows indicate cleavage sites of bacterial type III effector AvrRpt2.

(B) Immunoblot demonstrating similar expression levels of T7-epitope tagged wild type RIN4 and RIN4 missense mutant alleles in the *rpm1 rps2 rin4* background of transgenic lines used in this work. Immunoblot with α-T7 was performed on 30 µg of total proteins extract. The parental *rpm1 rps2 rin4* mutant was used as a negative control.

(C and D) Alignment of RIN4 orthologs from different plant species. RIN4 orthologs from 23 different plant species were selected and compared through Phytozome (www.phytozome.org). Amino acid alignment for RIN4 orthologs was conducted using Clustal W. (C) The conservation of threonine T20 (blue) and the very weak conservation of serine S47 (red) is indicated (blue and red arrow). (D) Red and blue arrows indicate conservation of putative phosphorylation site serine S141 (red), S160 (blue) and threonine T166 (blue) in *Arabidopsis thaliana* and other plants, respectively.

(E) Number of RIN4 orthologs presented in a phylogenetic tree of different sequenced organisms as found by the BLASTP search tool using *Arabidopsis thaliana* RIN4 protein sequence as query in phytozome v9.1 (www.phytozome.org).

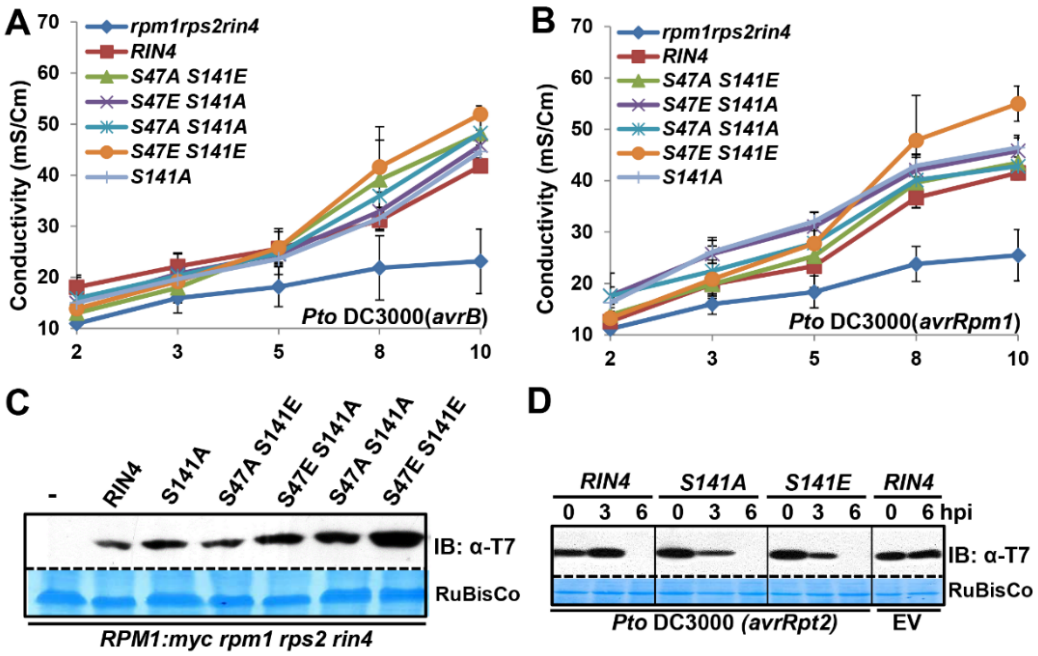

Figure S2, related to Figure 1. RIN4 S47 and S141 residues are dispensable for effector-dependent RPM1 activation.

(A, B) Conductivity assay for RPM1-mediated hypersensitive response (HR) in leaf-discs from transgenic *pRPM1::RPM1-myc rpm1 rps2 rin4* plants expressing T7-tagged wild type RIN4 or RIN4 missense mutant alleles as noted. Bacterial suspensions of 5 x 10^7 cfu / ml of either *Pto* DC3000(*avrB*) (A), or *Pto* DC3000(*avrRpm1*) (B), were infiltrated via hand inoculation into leaves from 5 week old plants. Ion-leakage was monitored starting 2 hours post bacterial infection. The *rpm1 rps2 rin4* triple mutant line serves as a negative control. Error bar represents 2 x SE.

(C) Immunoblot demonstrating similar expression levels of T7-epitope tagged wild type RIN4 and RIN4 missense mutant alleles in *pRPM1::RPM1-myc rpm1 rps2 rin4*. Immunoblot with α-T7 was performed on 30 µg of total proteins extract. The parental *pRPM1::RPM1-myc rpm1 rps2 rin4* mutant was used as a negative control (far left).

(D) Immunoblot with α-T7 to monitor RIN4 cleavage by AvrRpt2. Leaves from transgenic *rpm1 rps2 rin4* plants expressing indicated T7-tagged RIN4 derivatives were infiltrated with 5 x 10^7 cfu / mL of *Pto* DC3000(*avrRpt2*). 20 µg of total protein extract per time point was loaded followed by immunoblot with α-T7. Immunoblot with α-T7 infiltrated with *Pto* DC3000(EV) serves as a control for AvrRpt2-dependent cleavage of RIN4. Coomassie Brilliant Blue staining of RuBisCo demonstrates similar loading.

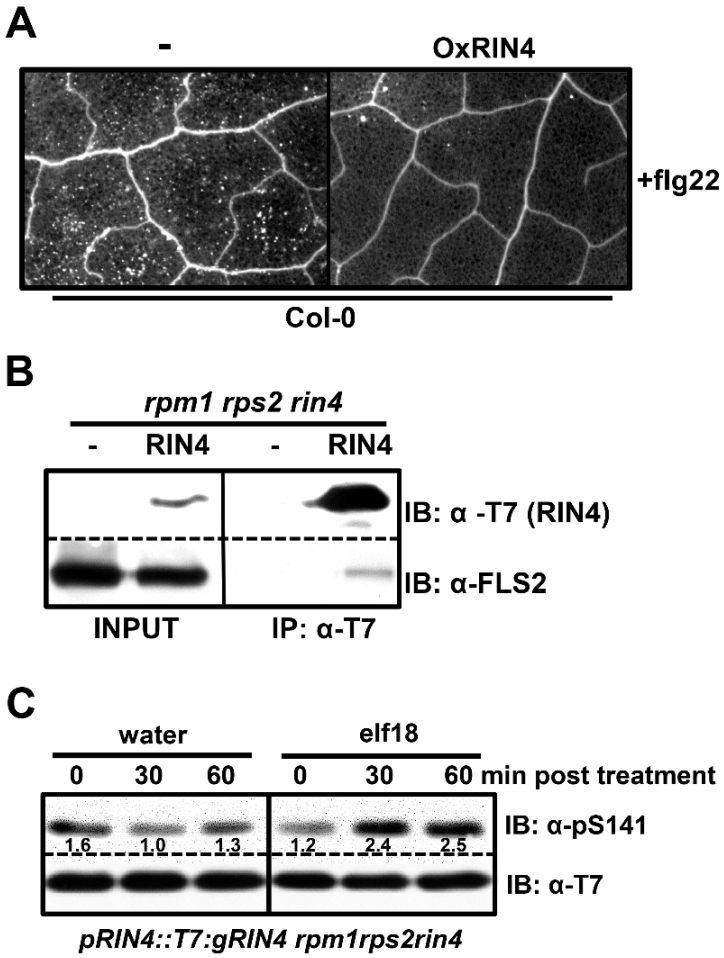

Figure S3, related to Figure 2. Suppressed callose accumulation in Col-0 and OxRIN4, association of RIN4 with FLS2 *in planta* and elf18-induced RIN4 S141 phosphorylation.

(A) Callose accumulation in Col-0 and OxRIN4 in Col-0 post flg22-treatment. Plants were treated with 1 µM flg22 48 hours post-treatment with 20 µM Dex to induce RIN4 expression in *Dex::RIN4* line. Samples were collected 12 hours post flg22-treatement followed by aniline blue staining to visualize callose. Two independent experiments displayed similar result.

(B) Co-immunoprecipitation of FLS2 with resting state wild type RIN4. Transgenic *pRIN4::T7-RIN4 rpm1 rps2 rin4* plants or parental controls were used for immunoprecipitation with α-T7. Co-immunoprecipitated FLS2 was detected by immunoblot with α-FLS2. Similar results were observed in two independent replicates.

(C) *pRIN4::T7-RIN4 rpm1 rps2 rin4* plants were hand infiltration with water (left) or 1 µM elf18 (right). Samples were collected 0, 30 and 60 min post elf18-treatment. 30 µg of total protein was loaded, followed by immunoblots with α-pS141 or α-T7 to monitor RIN4 phosphorylation on S141 residue and equal loading, respectively.

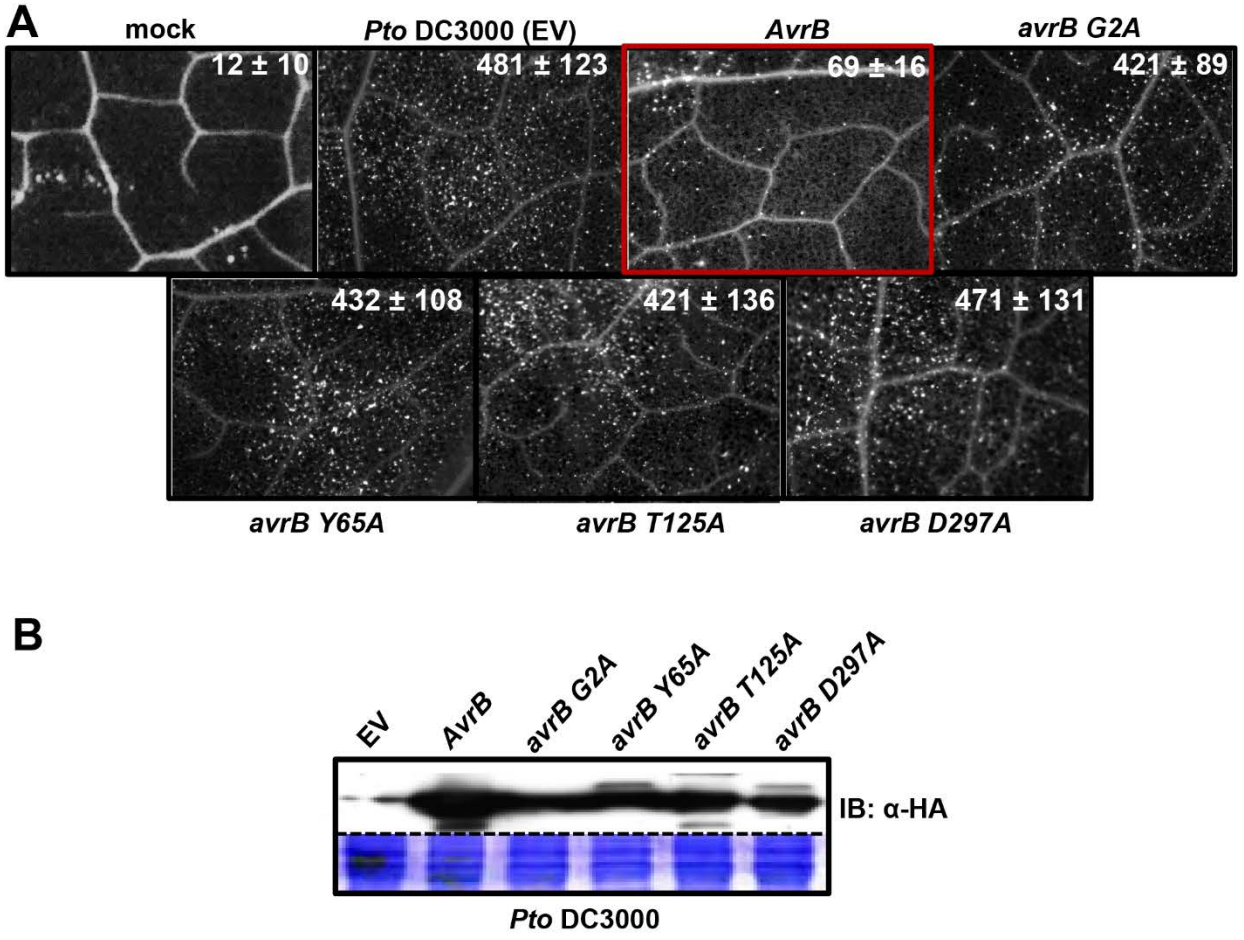

Figure S4, related to Figure 3. AvrB alleles that cannot activate RPM1 cannot suppress callose deposition induced by *Pto* DC3000.

(A) Induced callose deposits were counted 18 hours following inoculation with 5 x 10^7 cfu / ml *Pto* DC3000 bacteria expressing *avrB* or the indicated *avrB* missense mutants (Desveaux et al., 2007), into leaves of 5 week old transgenic *rpm1 rps2 rin4* plants expressing wild type T7-tagged RIN4. Counts are mean +/- 2 x SE based on 10 leave samples. Experiment was performed two times.

(B) Expression of HA-epitope tagged wild type and mutant AvrB alleles in *Pto* DC3000. Immunoblot with α-HA of 20 µg of total protein extract from bacteria confirms equal protein expression of the AvrB alleles.

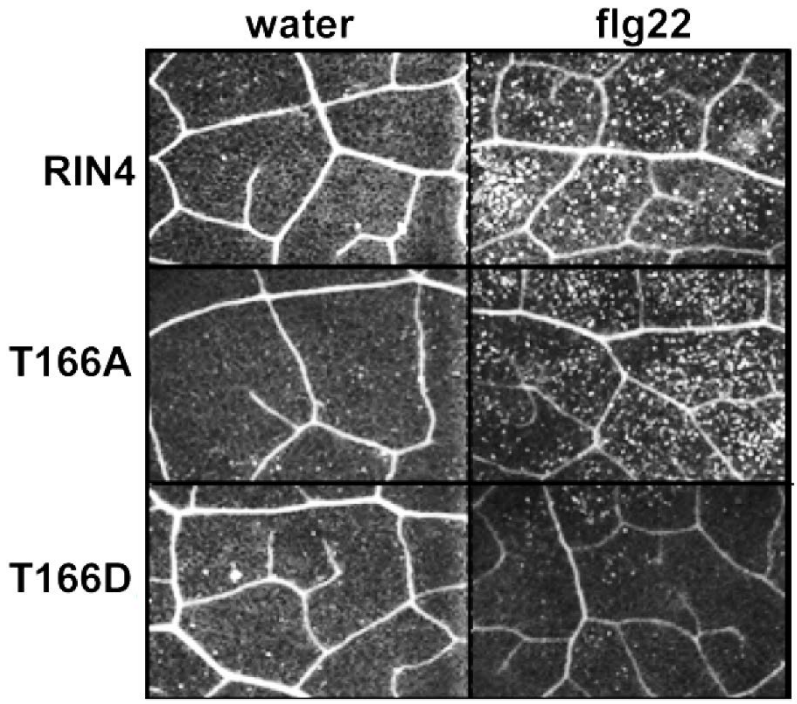

Figure S5, related to Figure 4. Phosphomimic RIN4 T166D blocks flg22 activated callose deposition. Each picture represents one of 16 leaves used for Figure 4C

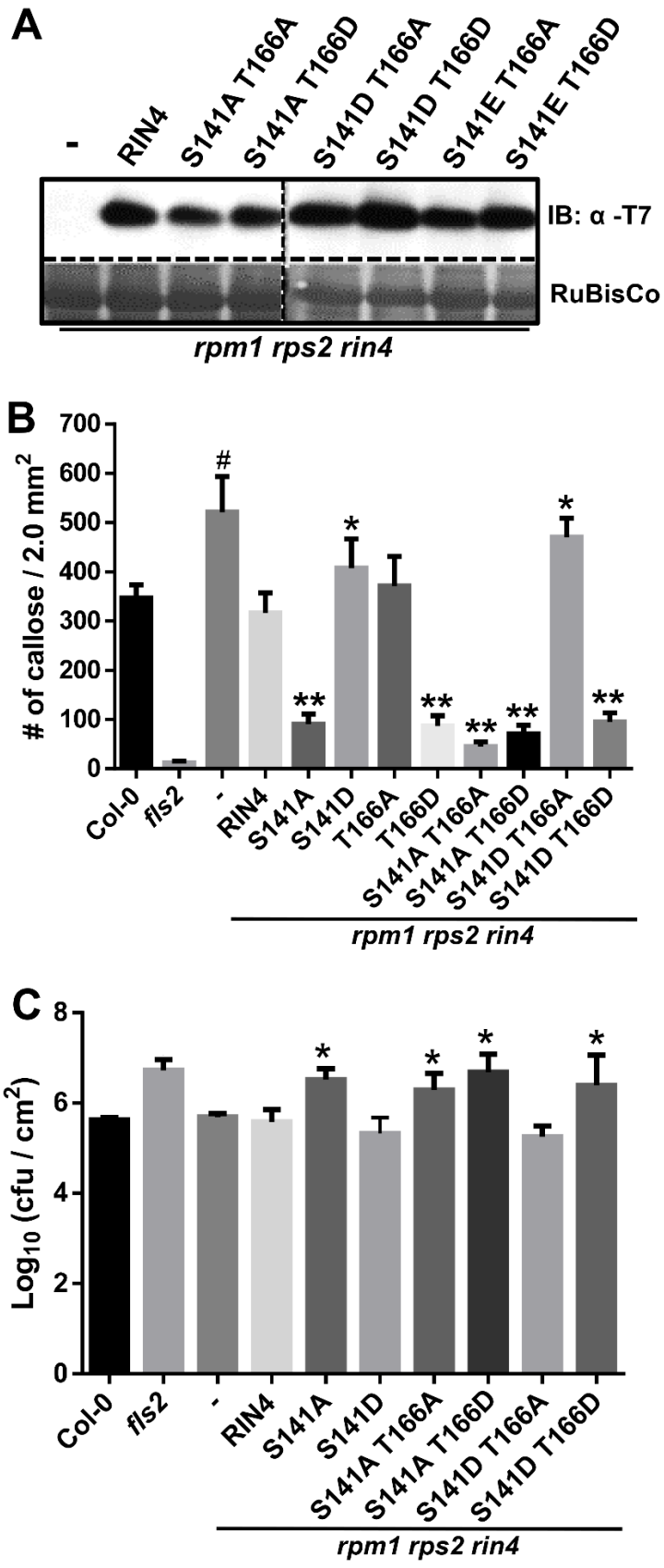
A
-
RIN4
S141A T166A
S141A T166D
S141D T166A
S141D T166D
S141E T166A
S141E T166D
IB: α -T7
RuBisCo
rpm1 rps2 rin4
B
# of callose / 2.0 mm2
700
600
500
400
300
200
100
0
#
*
**
Col-0
fls2
-
RIN4
S141A
S141D
T166A
T166D
S141A T166A
S141A T166D
S141D T166A
S141D T166D
rpm1 rps2 rin4
C
Log10 (cfu / cm2)
8
6
4
2
0
*
Col-0
fls2
-
RIN4
S141A
S141D
S141A T166A
S141A T166D
S141D T166A
S141D T166D
rpm1 rps2 rin4

Figure S6, related to Figure 5. MTI phenotypes in RIN4 S141D T166A and S141D T166D mutant.

(A) Transgenic *rpm1 rps2 rin4* plants expressing similar levels of *pRIN4 T7-RIN4*, or *RIN4 S141*- and *T166*-related *cis* double missense mutants confirmed by immunoblot using α-T7 antibody.

(B) Callose deposition in transgenic *rpm1 rps2 rin4* plants expressing T7-tagged wild type RIN4 and RIN4 missense mutants as indicated. The number of flg22-induced callose deposits was monitored as in Figure 5B. Number (#) sign denote significant difference compared to Col-0 using One-Way ANOVA test with Tukey-Kramer HSD with 95% confidence. Asterisks (* or **) demonstrate significant differences compared to RIN4 by One-Way ANOVA test with Tukey-Kramer HSD with 95% confidence.

(C) Flg22-activated bacterial growth suppression in transgenic *rpm1 rps2 rin4* plants expressing T7-tagged wild type RIN4 and RIN4 missense mutants as indicated. Leaves of 5 week old transgenic plants were pre-inoculated with 100 nM of flg22. Virulent bacteria *Pto* DC3000(EV) were inoculated 24 h later at 1 x 10^5 cfu / ml. Leaves were harvested for enumeration of bacteria 3 days later. Error bars represent 2 x SE (n = 4); the experiment was performed two times. For graphical clarity, data displayed here in S6B and S6C is derived from the same experiments shown in Figure 5B and 5C, respectively. The only difference is the exchange of data from transgenic lines expressing RIN4 S141D singly and in combinations (here) in place of data for lines expressing RIN4 S141E (Figure 5).

Table S1, related to Figure 1 and 5. Primers used in this study.

Primer	Sequence	Related experiment
5' RIN4 promoter primer Gateway	caaaaaagcaggctccGATCTGTCTTCTTTGATTTGA	cloning
3'RIN4 promoter primer with T7-tag	ACCCATTTGCTGTCCACCAGTCATGCTAGCCATGGGAGAGAGGTAGCTAAAGAA	Cloning
5' T7-tag with 5' RIN4 gDNA	ATGGCTAGCATGACTGGTGGACAGCAAATGGGTATGGCAGTAAGTGTTTTCTTTCC	Cloning
3' RIN4 primer Gateway	agaaagctgggtgCATTTTCCTCCAAAGCCAAAGCAGC	Cloning
RIN4 S47A forward	GACCCGGAGTATAACgCTGACTCTCAATCAC	Cloning
RIN4 S47A reverse	GTGATTGAGAGTCAGcGTTATACTCCGGGTC	Cloning
RIN4 S47E forward	GACCCGGAGTATAACgagGACTCTCAATCAC	Cloning
RIN4 S47E reverse	GTGATTGAGAGTCctcGTTATACTCCGGGTC	Cloning
RIN4 S141A forward	CTTAGAGCTGATGAAgcTCCTGAAAAAGTCAC	Cloning
RIN4 S141A reverse	GTGACTTTTTCAGGAgcTTCATCAGCTCTAAG	Cloning
RIN4 S141E forward	CTTAGAGCTGATGAAgagCCTGAAAAAGTCAC	Cloning
RIN4 S141E reverse	GTGACTTTTTCAGGctcTTCATCAGCTCTAAG	Cloning
RIN4 S141D forward	CTTAGAGCTGATGAAgacCCTGAAAAAGTCAC	Cloning
RIN4 S141D reverse	GTGACTTTTTCAGGgtcTTCATCAGCTCTAAG	Cloning
UBQ10 5'	AGATCCAGGACAAGGAGGTATTC	qRT
UBQ10 3'	CGCAGGACCAAGTGAAGAGTAG	qRT
At5g57220 5'	AATGGAGAGAGCAACACAATG	qRT
At5g57220 3'	ATACTGAGCATGAGCCCTTTG	qRT
At1g51890 5'	CCAGTTTGTTCTGTAATACTCAGG	qRT
At1g51890 3'	CTAGCCGACTTTGGGCTATC	qRT

SUPPLEMENTAL EXPERIMENTAL PROCEDURES

Vector construction

RIN4 and RIN4 derivatives were cloned as described (Chung et al., 2011). In brief, the *RIN4* promoter (*pRIN4*) consisted of 1.6kb upstream of the *RIN4* translational start codon. Genomic *RIN4* constructs were generated with gene-specific primers to incorporate a T7-epitope sequence directly at the N-terminus of *RIN4* (MASMTGGQQMG; ATG GCT AGC ATG ACT GGT GGA CAG CAA ATG GGT; Novagen) and using the native stop codon in the 3'-primer (Table S1). Full length genomic *RIN4* constructs with the native promoter and T7-epitope tag were cloned into the pDONR207 vector (Invitrogen, Carlsbad, CA). Expression clones for RIN4-related constructs were introduced into the pBAR1-GW destination vector (Chung et al., 2011) by LR reaction (Invitrogen, Carlsbad, CA).

Plants

Arabidopsis Col-0, isogenic mutants, transgenics expressing RIN4 wild type or RIN4 mutant derivatives were sown and grown as described (Boyes et al., 1998). To monitor MTI-responses we generated transgenic plants by transforming *rpm1 rps2 rin4* triple mutants. For ETI responses, the same constructs were transformed into the *RPM1-myc rpm1 rps2 rin4* (Chung et al., 2011). Dex-inducible RIN4 overexpression plants were generated in the previous study (Kim et al., 2005). The *bik1 pbl1* double mutant lines were obtained from C. Zipfel (Kadota et al., 2014).

Bacteria

Bacterial strains for *Pto* DC3000(EV), *Pto* DC3000(*avrB*) and *Pto* DC3000(*avrRpt2*) were maintained and grown as described in Chung et al., (2011). *Pto* DC3000(*HopF2*^{ATG}) was provided by Darrell Desveaux. In brief, HopF2^{ATG} from *P. syrinage* pv. *tomato* was cloned into the multicopy plasmid pBBR2 MCS-2 with 100 base-pair upstream including the SchF ATG start codon followed by transformation into *hopF2*-mutated *Pto* DC3000 (Wilton et al., 2010; Wu et al., 2011).

Protein extraction, immunoblot and co-immunoprecipitation analyses

To monitor the expression of proteins in transgenic Arabidopsis plants, two leaves of similar size from independent Arabidopsis transgenic lines were harvested and ground in liquid nitrogen. Total plant crude extracts were prepared with 150 µL of grinding buffer (20 mM Tris-HCl pH 7.5, 150 mM NaCl, 1% Triton X-100, 1 mM EDTA pH 8.0 and 0.1% SDS) also containing 10 mM DTT and

1X plant protease inhibitor cocktail (Sigma-Aldrich). The lysates were centrifuged at 14,000 rpm for 10 min at 4ºC. Supernatants were collected and the protein concentration was determined with the BioRad Bradford quantification method (BioRad). Protein extracts were electrophoresed through 8% for FLS2, 10% for MPKs or 14% SDS-PAGE for RIN4 followed by transfer with the semi-dry method (Thermo Scientific) onto PVDF membrane (GE Healthcare). Immunoblots were performed with a 1:5000 dilution of α-T7-HRP (Novegen), 1:2000 dilutions of α-pS141 (Genscript), α-pERK (Cell Signaling) or α-FLS2 (a kind gift of C. Zipfel; (Roux et al., 2011), and 1:2000 dilution of α-MPK6 (Sigma). Endogenous RIN4 was detected by immunoblot of α-RIN4 with 1:2000 dilutions of α-RIN4 antisera (Genscript). Blots were incubated with HRP-conjugated secondary antibody and detected by ECL or ECL plus following the manufacturer's directions (GE Healthcare). For Immunoblots with α-pS141 or α-pT166, plant total proteins were extracted with 200 µL of grinding buffer with 1 X phosphatase inhibitor cocktail (Thermo Scientific). Proteins were transferred onto PVDF membrane (GE Healthcare) followed by blocking and incubation with antibody in 5 % BSA. Primary antibody incubation with α-pS141 or α-pT166 was fulfilled overnight at 4 ˚C followed by 1 hour secondary antibody as described above. Co-immunoprecipitation between FLS2 and either wild type or mutant RIN4 proteins was performed as described in the previous study (Chung et al., 2011). For protein quantification of RIN4 pS141, all band intensities were measured using ImageJ (NIH). The density of the pS141 bands was generated relative to loading control from immunoblot with α-T7 in Figure 4D or with α-RIN4 in Figure 2E. The density of each signal from immunoblot with α-T7 or with α-RIN4 were normalized to the higher density. Individual pS141 band was measured and re-calculated according to normalization of α-T7 or α-RIN4 immunublot.

Quantification of hypersensitive response (HR) *in planta*

RPM1-dependent HR triggered by *Pto* DC3000(*avrB*) and *Pto* DC3000(*avrRpm1*) was visualized by trypan blue staining and quantified by conductivity measurement (Boyes et al., 1998; Chung et al., 2011; Mackey et al., 2002). Bacteria suspensions from *Pto* DC3000 either expressing AvrB or AvrRpm1 were prepared and infiltrated at a concentration of 5×10^7 cfu/mL (Boyes et al., 1998). To measure the conductivity from infiltrated leaves, three replicates of four leaf discs each were collected and submerged into 6 mL of double distilled water, and conductivity measured (Orion, model 130) at the indicated time points.

REFERENCES

Boyes, D.C., Nam, J., and Dangl, J.L. (1998). The Arabidopsis thaliana RPM1 disease resistance gene product is a peripheral plasma membrane protein that is degraded coincident with the hypersensitive response. Proceedings of the National Academy of Sciences of the United States of America *95*, 15849-15854.

Chung, E.H., da Cunha, L., Wu, A.J., Gao, Z., Cherkis, K., Afzal, A.J., Mackey, D., and Dangl, J.L. (2011). Specific threonine phosphorylation of a host target by two unrelated type III effectors activates a host innate immune receptor in plants. Cell host & microbe *9*, 125-136.

Kadota, Y., Sklenar, J., Derbyshire, P., Stransfeld, L., Asai, S., Ntoukakis, V., Jones, J.D., Shirasu, K., Menke, F., Jones, A.*, et al.* (2014). Direct regulation of the NADPH oxidase RBOHD by the PRR-associated kinase BIK1 during plant immunity. Molecular cell *54*, 43-55.

Mackey, D., Holt, B.F., 3rd, Wiig, A., and Dangl, J.L. (2002). RIN4 interacts with Pseudomonas syringae type III effector molecules and is required for RPM1-mediated resistance in Arabidopsis. Cell *108*, 743-754.

Roux, M., Schwessinger, B., Albrecht, C., Chinchilla, D., Jones, A., Holton, N., Malinovsky, F.G., Tor, M., de Vries, S., and Zipfel, C. (2011). The Arabidopsis leucine-rich repeat receptor-like kinases BAK1/SERK3 and BKK1/SERK4 are required for innate immunity to hemibiotrophic and biotrophic pathogens. The Plant cell *23*, 2440-2455.

Wilton, M., Subramaniam, R., Elmore, J., Felsensteiner, C., Coaker, G., and Desveaux, D. (2010). The type III effector HopF2Pto targets Arabidopsis RIN4 protein to promote Pseudomonas syringae virulence. Proceedings of the National Academy of Sciences of the United States of America *107*, 2349-2354.

Wu, S., Lu, D., Kabbage, M., Wei, H.L., Swingle, B., Records, A.R., Dickman, M., He, P., and Shan, L. (2011). Bacterial effector HopF2 suppresses arabidopsis innate immunity at the plasma membrane. Molecular plant-microbe interactions : MPMI *24*, 585-593.